NASA CR-159164

(NASA-CR-159164) THERMOPHYSICAL PROPERTIES DATA ON GRAPHITE/POLYIMIDE COMPOSITE MATERIALS Final Report (General Dynamics/Convair) 69 p HC A04/MF A01 CSCL 11D G3/24

N80-14197

Unclas 46484

THERMOPHYSICAL PROPERTIES DATA ON GRAPHITE/POLYIMIDE COMPOSITE MATERIALS

M. D. CAMPBELL
D. D. BURLEIGH

GENERAL DYNAMICS CONVAIR DIVISION
P.O. BOX 80847, MZ 43-6332
SAN DIEGO, CALIFORNIA 92138

CONTRACT NAS1-15103

NOVEMBER 1979

National Aeronautics and Space Administration

Langley Research Center
Hampton, Virginia 23665

ABSTRACT

Experimental data for the thermal conductivity, thermal expansion, specific heat, and emittance of [0] and $[0, 45, 90, 135]_S$ laminates of HTS/NR 150B2 and HTS/PMR 15 are presented. Measurements were made over the temperature range 116K to 588K (-250F to 600F).

Results for the two materials were similar with some differences attributable to laminate quality. Higher expansion coefficients for the HTS/PMR 15 specimens in the resin-dominated directions indicate a higher coefficient for PMR 15 than NR 150B2.

THERMOPHYSICAL PROPERTIES DATA ON GRAPHITE/POLYIMIDE COMPOSITE MATERIALS

Malcolm D. Campbell and Douglas D. Burleigh

General Dynamics, Convair Division

SUMMARY

Measurements of the thermal properties of HTS/NR 150B2 and HTS/PMR 15 laminates were made over the temperature range 116K to 588K (-250°F to 600°F). Properties investigated included thermal conductivity, thermal expansion, specific heat and emittance. Layups of [0] and $[0, 45, 90, 135]_S$ were measured in two directions for both materials.

Both materials produced somewhat poorer quality laminates than generally achievable with lower temperature resins such as epoxies. This is typical of these systems at this time. It was expected that, for a given layup and direction, results would be comparable for the two materials. In general, this was the case with some differences attributable to laminate quality rather than differences in basic materials properties. However, higher expansion coefficients for the HTS/PMR 15 specimens in the resin-dominated directions indicate a higher coefficient for PMR 15 than NR 150B2. Erratic variations in thermal expansion results from the same specimen were observed at times. Although these were tentatively attributed to laminate quality, additional work is necessary to fully understand this behavior.

INTRODUCTION

Graphite fiber reinforced polyimide composites are a potential solution to the need for high temperature organic matrix composites for aerospace applications. Being relatively new in the world of composites, their thermal properties are not well known.

The purpose of this program was to conduct a preliminary investigation of the thermal expansion, thermal conductivity, specific heat and emittance of two prominent graphite/polyimides. [1]

The work was performed in the Physical Properties Laboratories at General Dynamics Convair Division's Kearny Mesa Plant, San Diego, CA and was sponsored by NASA Langley Research Center under Contract No. NAS-1-15103.

The NASA Technical Monitor was Dr. Ronald K. Clark; Program Manager was Malcolm D. Campbell.

[1] Certain commercial materials are identified in this report in order to specify adequately which materials were investigated in the research effort. In no case does such identification imply recommendation or endorsement of the product by NASA, nor does it imply that the materials are necessarily the only ones or the best ones available for the purpose.

TEST MATERIALS

Measurements were made on two materials, each in a [0, 45, 90, 135] quasi-isotropic layup and in a unidirectional layup.

The HTS/PMR 15 panels were furnished to the program by NASA Langley Research Center. The HTS/NR 150B2 panels were fabricated by General Dynamics, Convair Division. As a check of laminate quality, resin content and tensile strength were measured for both layups of both materials. Results are shown in Table 1.

Figures 1 shows cross sections of both layups of both materials at 20x. These were all taken from thermal expansion specimens after testing. Both materials showed extensive microcracking in the quasi-isotopic layup. Samples of untested material (no thermal cycle exposure) were also examined and appeared similar. Void content of the HTS/PMR 15 panels was low; void content was high in the HTS/NR 150B2 panels.

Compared to laminates made with lower temperature resins such as epoxies, individual plies in both materials wandered considerably. The photos in Figure 1 show areas where the plies are significantly unparallel. It is assumed that this effect is caused by the relatively poor impregnation of the yarn by the matrix in the pre-preg, i.e., the resin is lying on the surface of the yarn rather than being homogeneously distributed with the fibers.

Table 1. Test Panel Properties

I.D.	Material	Layup	Plies	Nominal Thickness (mm)	Resin Content (Wt. %)	Tensile Strength (MN/m^2)
Clark 1	HTS/PMR 15	$[0]_{18}$	18	3.2	35.1	1263.
Clark 3	HTS/PMR 15	$[0,45,90,135]_{2S}$	16	2.8	32.9	460.
C544	HTS/NR 150B2	$[0]_{24}$	24	3.2	22.2	1551.
C545	HTS/NR 150B2	$[0,45,90,135]_{S3}$	24	3.2	23.1	548.

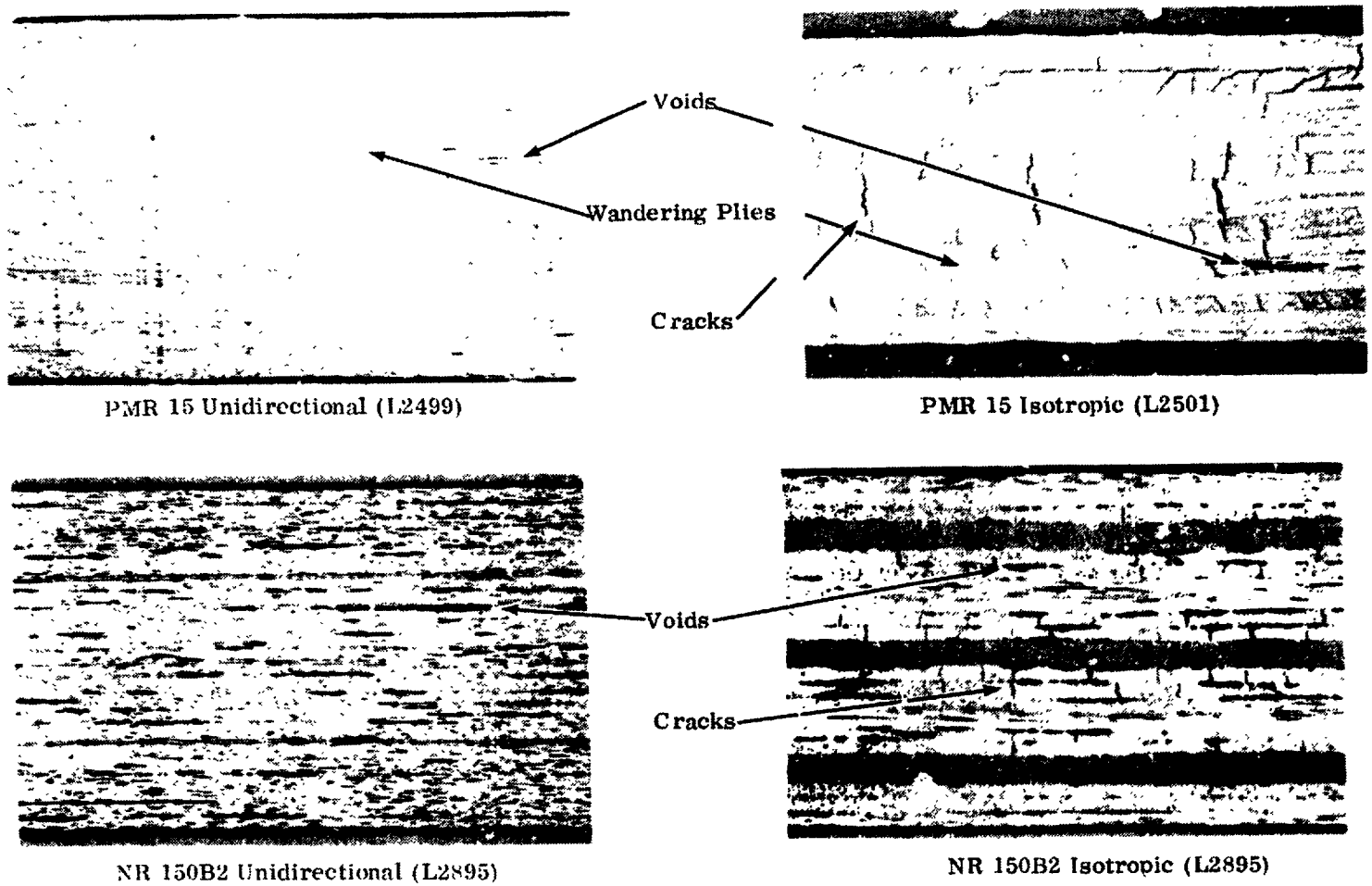

Figure 1. Test Laminate Cross Sections (20X)

TEST MATRIX AND METHODS

Table 2 shows a matrix of the tests performed. Designations of test directions correspond to those commonly used to designate principle axes of a laminate, i.e., X is parallel to the planes of the plies and in the direction of the 0° fibers; Y is parallel to the planes of the plies and normal to the 0° fibers; Z is normal to the plies.

Thermal Conductivity

Differences in thermal conductivities of the materials between test directions parallel to and across the high conductivity graphite fibers required two test methods. The high conductivities were in the X directions of both the unidirectional and quasi-isotropic layups. Conductivities were low in the Y direction of the unidirectional layups and in the Z direction of the isotropic layups.

For the X directions, the cut strip apparatus shown in Figures 2 and 3 was used. In this method, a test specimen is built up from alternate strips of the material under test and a standard material. One end of the stack is attached to a heat sink through an electrically heated plate. A second heater is attached to the free end. Thermocouples are installed in each segment. The entire assembly is radiation-shielded and maintained in a high vacuum to minimize heat losses. The heat sink is cooled by LN_2.

Measurements are made by establishing the desired mean temperature and a temperature differential of approximately 6 to 20K across the stack with the two heaters. When equilibrium is reached, the temperature differences across the specimen and the standards are recorded.

Thermal conductivity is then calculated using the relationship:

$$K_x = K_s (\Delta T_s/\Delta T_x)(X_x/X_s)(A_x/A_x)$$

where

K_x = thermal conductivity of test material

K_s = thermal conductivity of standard material

ΔT_s = temperature difference across standards (average of two)

ΔT_x = temperature difference across test specimen

X_s = distance between thermocouples on standards (average of two)

Table 2. Test Matrix

Material (Layup)	Thermal Conductivity (116 to 588K)*			Thermal Expansion (116 to 588K)			Specific Heat (116 to 588K)	Emittance (300 and 588K)
	X	Y	Z	X	Y	Z		
HT-S/NR150B2 (Unidirectional)	1	1		2	2			
HT-S/NR150B2 (Quasi-Isotropic)	1		1	2		2	2	2
HT-S/PMR15 (Unidirectional)	1	1		2	2			
HT-S/PMR15 (Quasi-Isotropic)	1		1	2		2	2	2

*Temperature extremes are: 116, 588K; -157, 316C; -250, 600F.

Numbers indicate specimen quantities

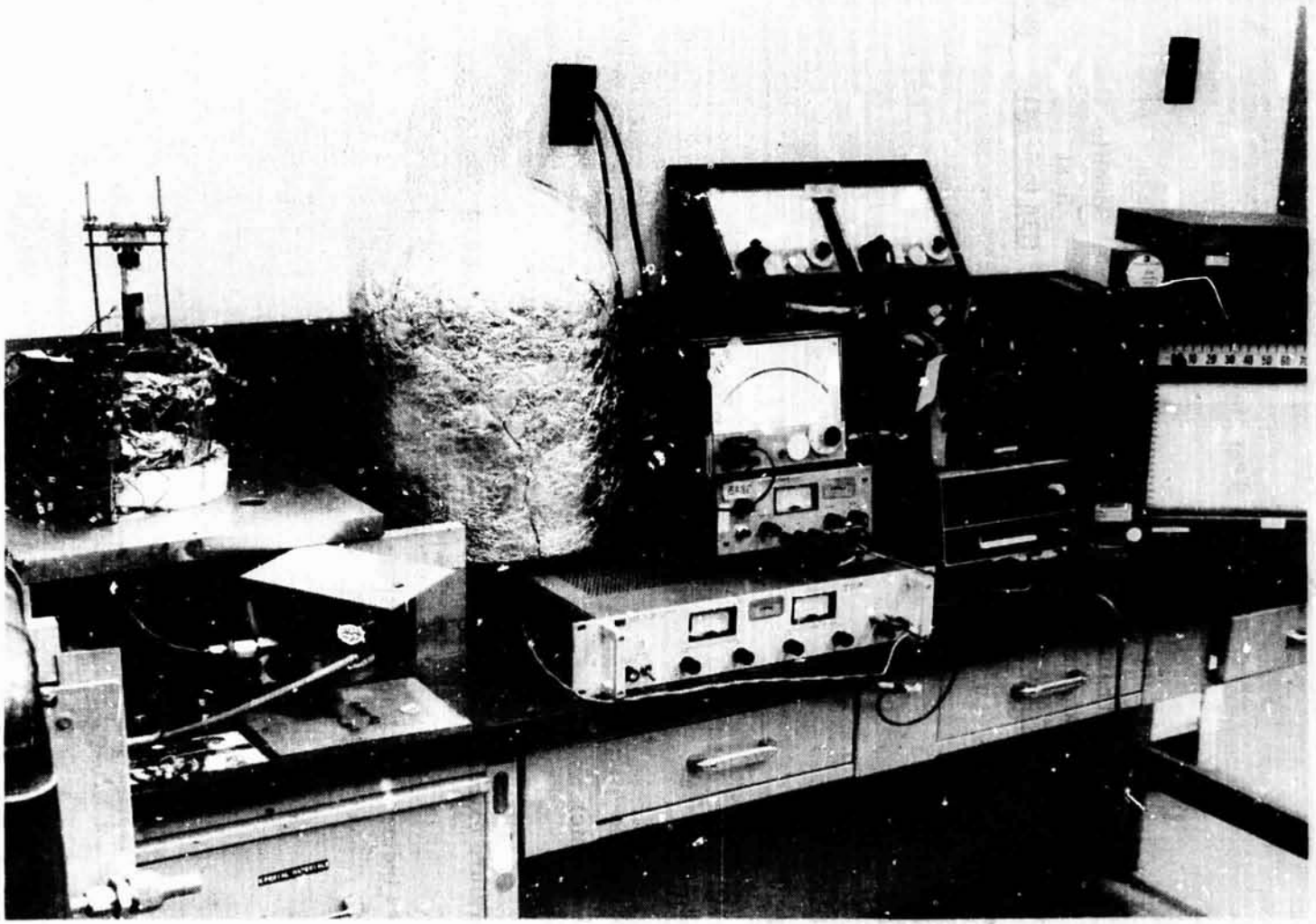

Figure 2. Cut Strip Thermal Conductivity Apparatus

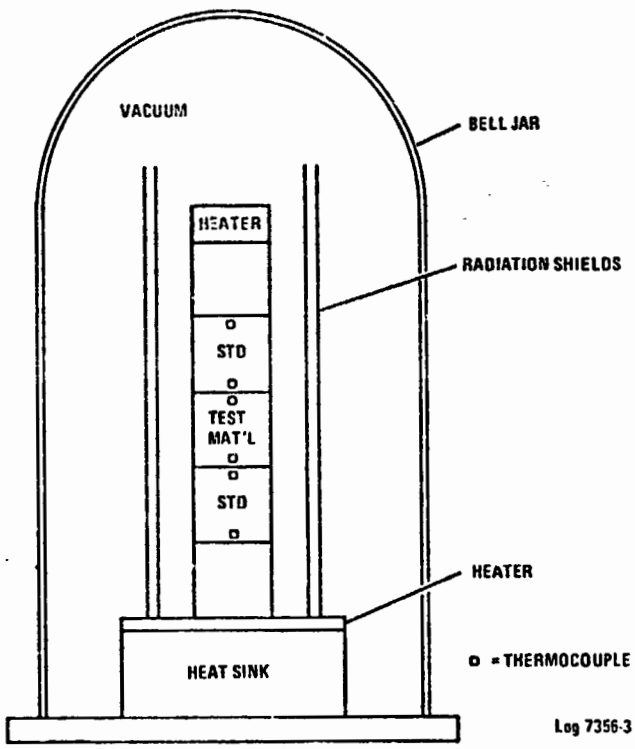

Figure 3. Schematic of Cut Strip Thermal Conductivity Apparatus

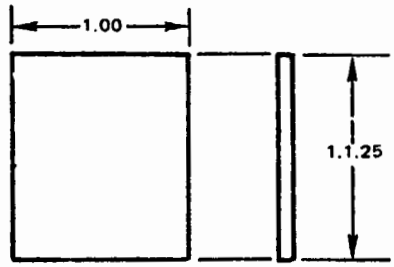

Figure 4. Cut Strip Specimen Configuration

X_x = distance between thermocouples on test specimen

A_s = cross-sectional area of standards (average of two)

A_x = cross-sectional area of test specimen

The test specimen configuration is shown in Figure 4. Standards for each measurement were chosen to produce ΔT's comparable to those across the test material to minimize errors due to unequal heat losses. Standards were machined from 321 steel certified and calibrated by NBS. Overall accuracy of the measurement is estimated to be within ±5% over the full temperature range.

Thermal conductivity data was taken at mean temperatures of approximately 116, 180, 245, 310, 375, 440, 505 and 569K.

Measurements in the low conductivity directions were made on a guarded hot-plate apparatus shown in Figures 5 and 6. This is an absolute method which determines thermal conductivity directly without the use of standards and is covered in principle by ASTM C177.

In this method, two thin concentric electrical heaters are sandwiched between two test panels. The test panels are approximately 100 mm in diameter with the center 50 mm diameter used as the test section. The specimens are instrumented with thermocouples so that their temperatures may be monitored. The specimens are in contact with heat sinks at their outer faces. The heaters and heat sink are adjusted to bring the center section to the desired mean temperature and ΔT. The power to the guard heater is adjusted to eliminate lateral gradients and to assure that all power supplied to the center heater flows normal to the sample planes.

At equilibrium the electrical power to the center heater and the average hot and cold face temperatures are recorded. Thermal conductivity, K, is calculated from the relationship

$$K = C_1 \cdot (EI) \cdot t/A \cdot \Delta T$$

where:

C_1 = Geometry and unit factor

(EI) = Center heater power

t = Average center-section thickness

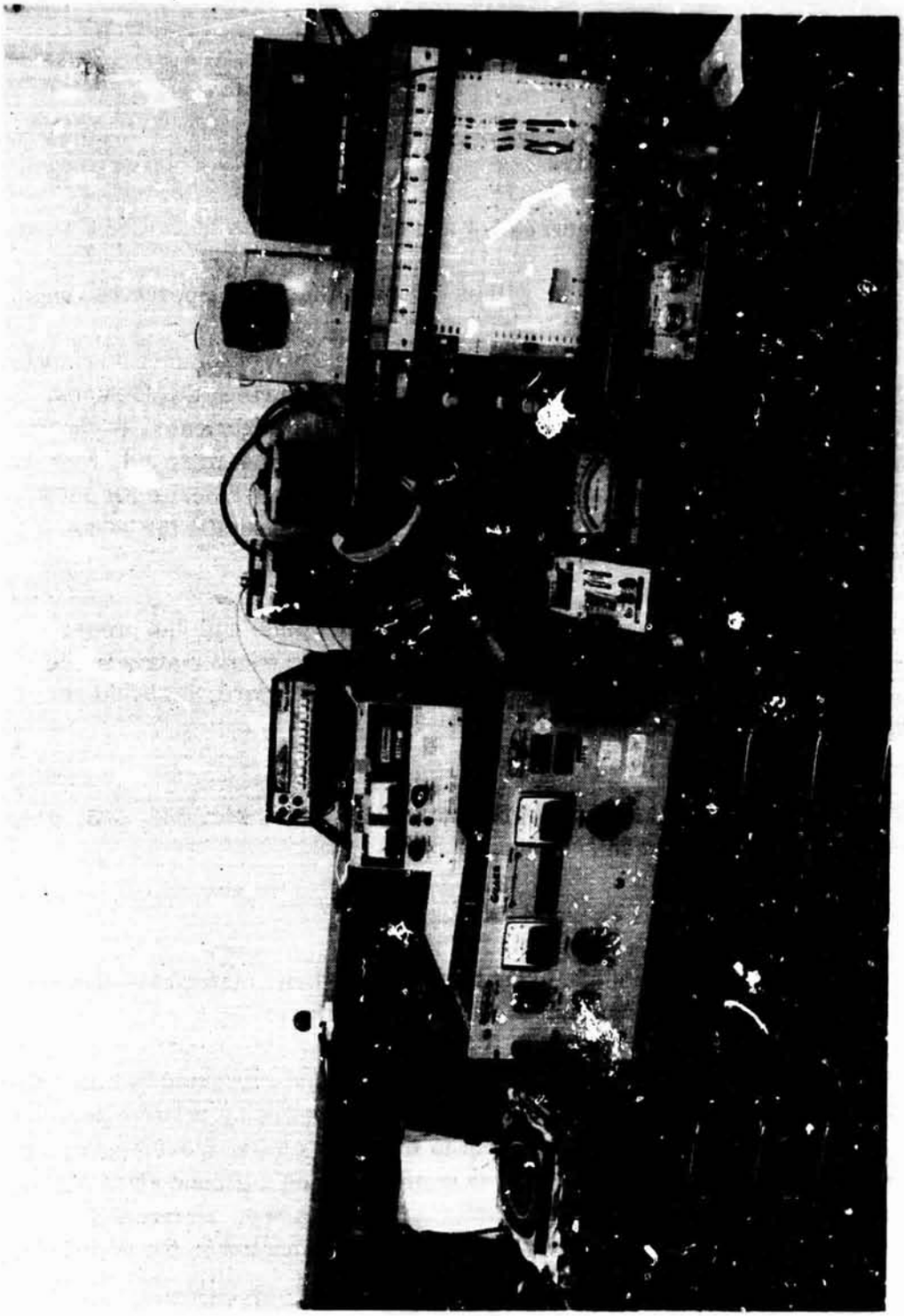

Figure 5. Guarded Hot Plate Thermal Conductivity Apparatus

A = Effective center-section area

ΔT = Temperature difference between hot and cold faces

Accuracy of the method is estimated to be within ±5% over the full temperature range.

The sample configurations are shown in Figure 7. For the Z direction measurements, 100 mm discs were cut from the as-received sheet without disturbing the surfaces. The Y direction measurements were made using specimen discs fabricated as shown in Figure 7b. Thirty-two strips of approximately 100 mm by 4 mm were cut, with the 4 mm dimension in the Y direction. These were then bonded with Fiberite NR 150B2 resin to form a plate with the laminate Y direction oriented through the thickness. The 100 mm test discs were then cut from these plates.

This procedure provided a test specimen for the guarded hot plate with the proper orientation. The resin film has a thermal conductivity similar to the matrix in the laminates and amounted to less than 1% of the total area. Therefore, it should not substantially influence the test results.

Data was taken at mean temperatures of approximately 116, 180, 245, 310, 375, 440, 505 and 588K for each test specimen set.

Thermal Expansion

All expansion measurements were made using the modified Leitz diatometer shown in Figures 8 and 9 and the specimen configurations shown in Figure 10.

In this apparatus, the specimen is contacted at each end by and supported by concentric fused silica tubes. The relative length of a specimen is indicated by relative positions of the tubes. Movement of one tube with respect to the other causes movement of a prism, which results in vertical deflection of a light beam projected on a ground glass plate. Specimen length changes are magnified by a factor as large as 800. Horizontal deflection of the light beam is controlled by a thermocouple mounted on the specimen.

The specimen is maintained in a dry helium atmosphere. Temperature of the specimen is varied by varying the power setting of the furnace. The furnace used for low temperatures is shown in both figures. It operates in a liquid nitrogen environment, and has a range of 80K to 475K. For this investigation, this furnace was used from 144K to 297K. A high temperature wire-wound furnace was used from 297K to 589K.

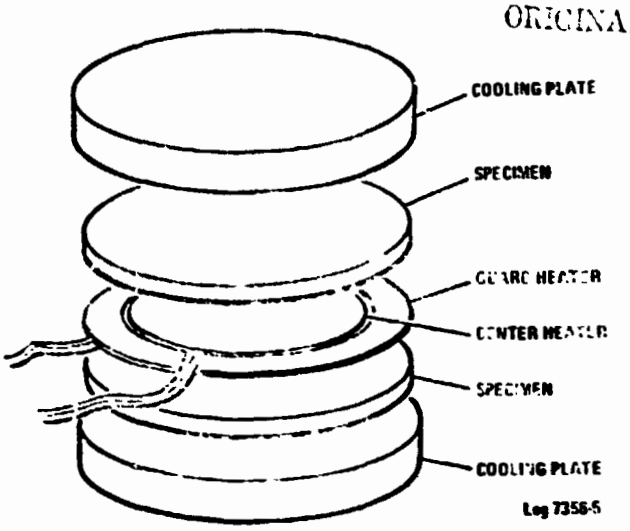

Figure 6. Schematic of Guarded Hot Plate Thermal Conductivity Apparatus

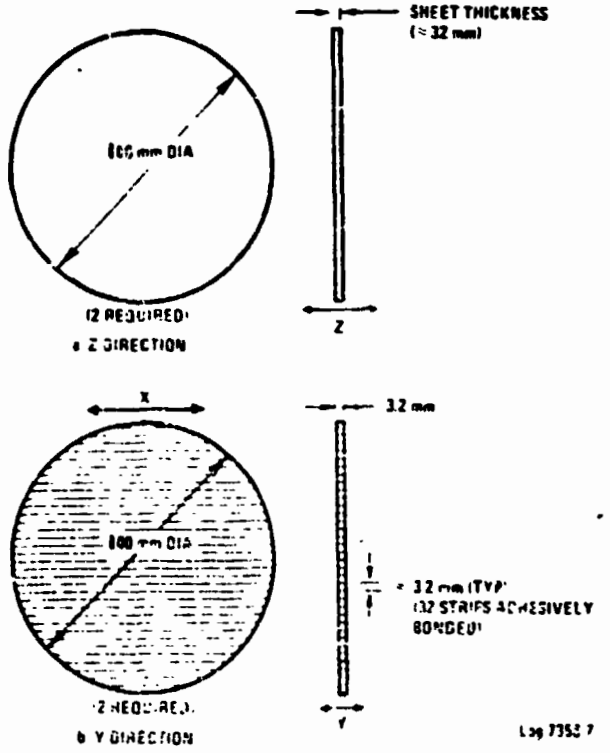

Figure 7. Guarded Hot Plate Specimen Configurations

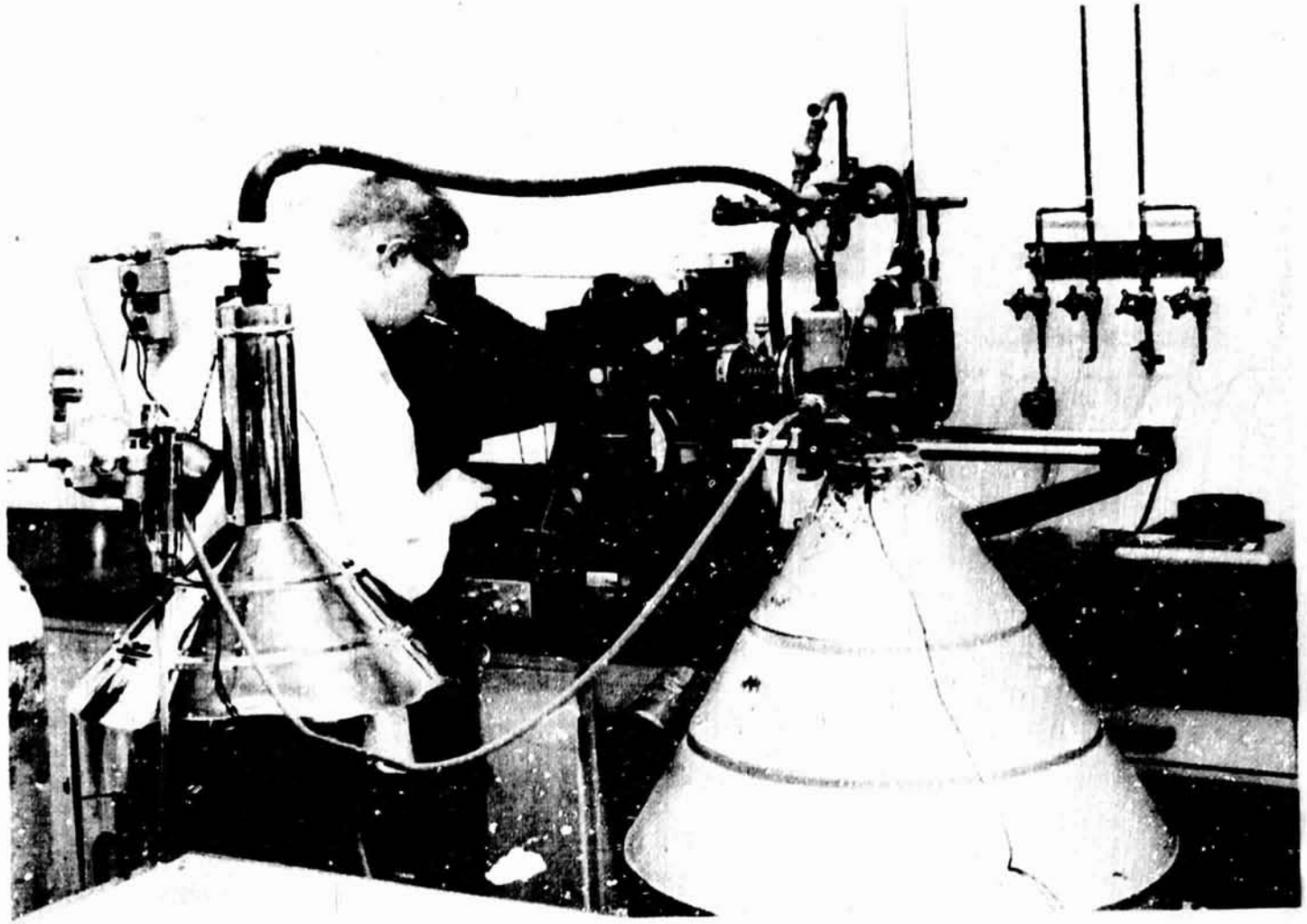

Figure 8. Modified Leitz Dilatometer

Power changes necessary to achieve the desired specimen temperature were made, and the specimen was permitted to come to thermal and structural equilibrium. Temperatures were changed approximately every 10 to 20 minutes. When equilibrium was reached, vertical displacement of the light beam and specimen temperature were recorded, and the power set for the next desired temperature. Displacement was hand marked on the glass plate.

At the conclusion of a run, the specimen displacement data was read using a calibrated traveling telescope, converted to $\Delta l/l$ with respect to the original reference length at ambient temperature, and plotted as a function of temperature.

The apparatus is routinely calibrated using an NBS-certified fused-silica standard. Accuracy over the full temperature range is better than $\pm 7 \times 10^{-6}$ m/m. This in a mean coefficient uncertainty of $\pm 0.016 \times 10^{-6}$ m/m/K (0.009×10^{-6} in/in/F) over 473K (850F).

For the X and Y directions, a 50.8 mm length in the test direction was used. For the Z direction, the original sheet thickness (3.2 mm) was used (Figure 10). Because of the high expansion in the Z direction, the short sample did not compromise the accuracy. To eliminate the possibility of length changes due to changes in moisture content during the expansion test, all specimens were vacuum-dried and desiccant-stored prior to test. For all specimens Δl data was taken at the following temperatures in sequence: 297, 116, 176, 236, 297, 347, 397, 447, 497, 547, 588, 297, 116, 588, 297K. This resulted in two complete cycles from room temperature to cryogenic temperatures to elevated temperatures and back to room temperature.

Specific Heat

Specific heats were measured using the DuPont 910 Differential Scanning Calorimeter shown in Figures 11 and 12. In this apparatus, a reference pan and a sample pan containing a small test specimen are equilibrated at the lowest temperature of interest, and then heated through the temperature range of interest. The apparatus is constructed to supply the same heat input to both pans at all times. As the two pans heat, the ΔT between them is recorded. This ΔT is used to calculate the specific heat of the unknown at any temperature through which the cell is heated. With proper calibration using an NBS-certified synthetic sapphire standard, uncertainties in the results are held to less than ±2%.

For this program, data were taken over the temperature range 116K to 588K. Specific heats of each sample were calculated at 116, 180, 245, 310, 375, 440, 505 and 588K and plotted against temperature.

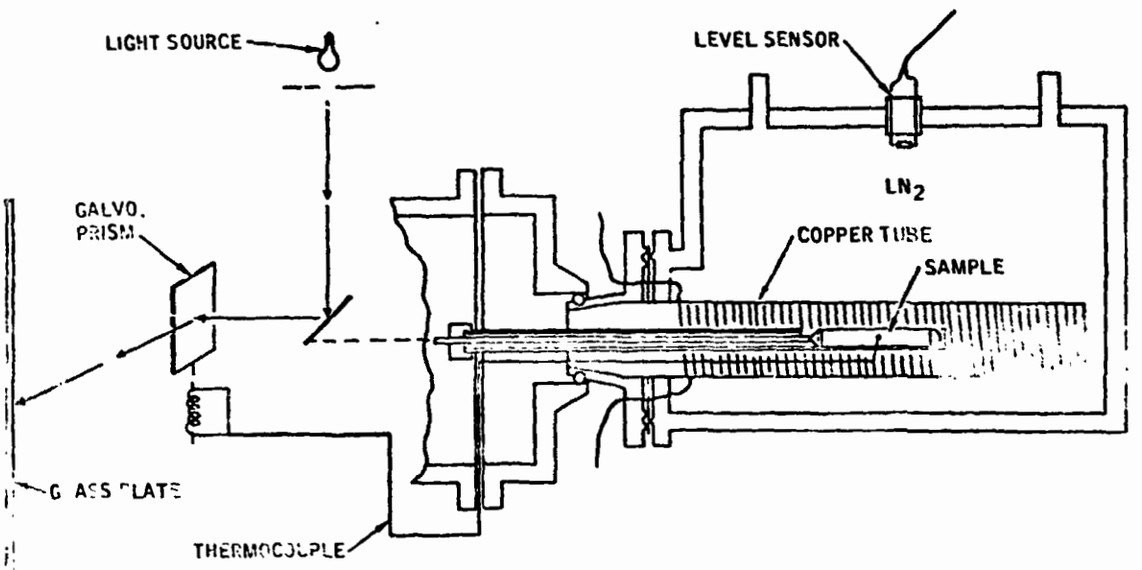

Figure 9. Schematic of Modified Leitz Dilatometer

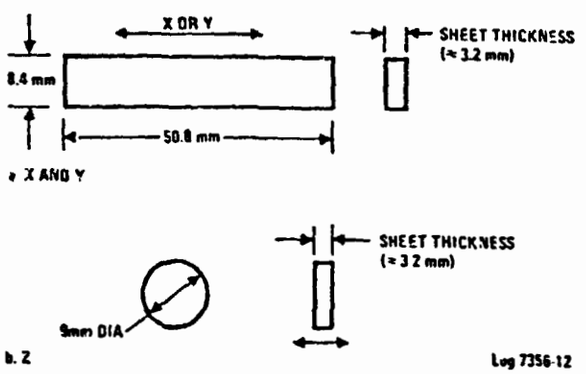

Figure 10. Thermal Expansion Specimen Configurations

Figure 11. Differential Scanning Calorimeter

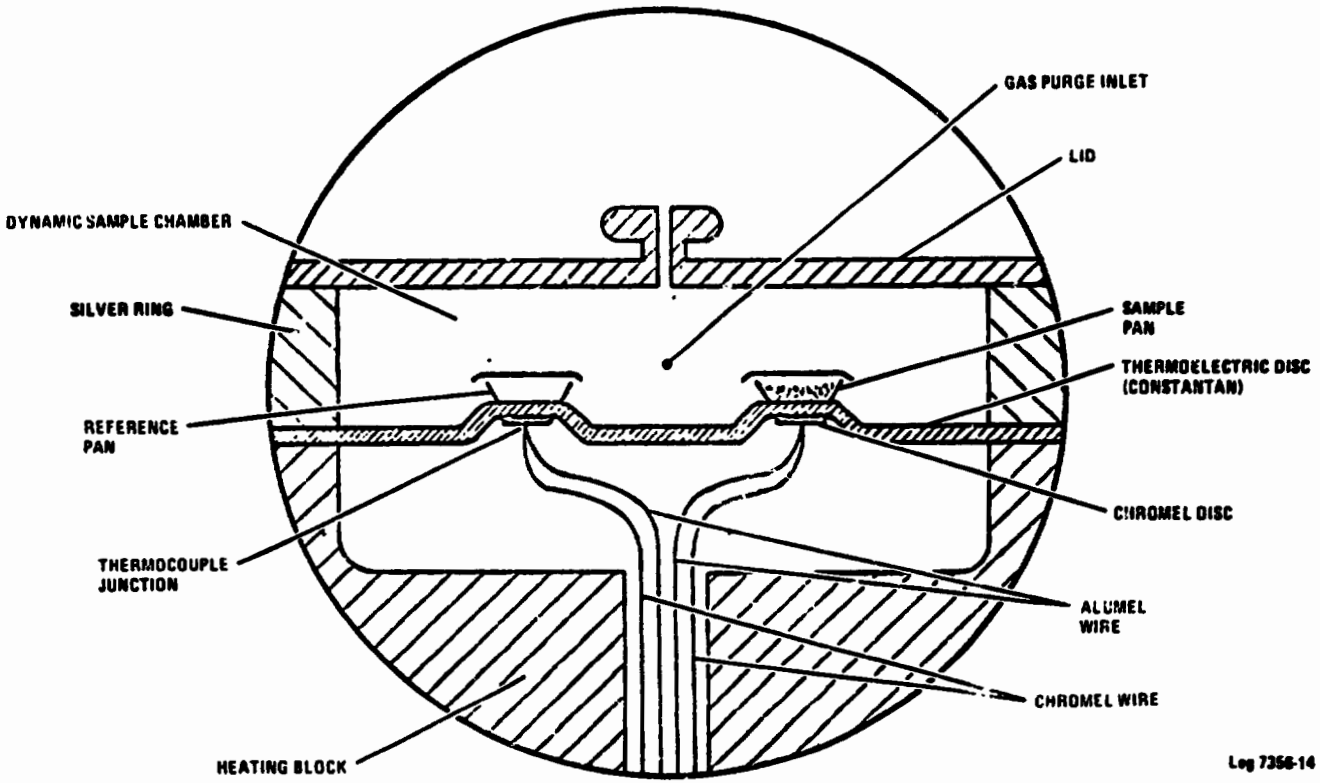

Figure 12. Schematic of Specific Heat Test Cell

A test specimen approximately 1 mm x 6 mm diameter was used. Test specimens were vacuum-oven dried prior to test so that the energy necessary to drive off the water was not included in the specific heat measurement.

Emittance

Total hemispherical emittance was obtained by measuring spectral reflectivity and using the relationship:

$$\rho_\lambda + \epsilon_\lambda = 1$$

where

ρ_λ = spectral reflectivity, and

ϵ_λ = spectral emissivity.

Spectral reflectivity measurements were made at ambient from 2.5 to 30 μm using an ellipsometer (Figures 13 and 14). The emittance, ϵ, was then calculated at ambient and 588K as follows:

$$\epsilon_T = \frac{\int_{\lambda_1}^{\lambda_2} (1 - \rho_\lambda) N_{\lambda T} \, d\lambda}{\int_{\lambda_1}^{\lambda_2} N_{\lambda T} \, d\lambda}$$

where $N_{\lambda T}$ is the Planck blackbody radiation function.

Figure 13 shows the optical system of the ellipsometer. The pyrex ellipsoid has a highly polished inner surface upon which a film of aluminum has been evaporated. It has a semi-major axis of 15.2 cm and a semi-minor axis of 15.0 cm, with foci 50.8 mm apart. The source is placed on the semi-major axis with its center at one focus; the sample is centered at the other focus, as shown in Figure 13. The focusing characteristics of the ellipsoid are such that a point source of light emanating from one focus is imaged at the other. Using a properly sized radiation source, the sample is uniformly illuminated over a hemisphere of 2 π steradians.

The source system - including the source, ellipsoid, sample holder, and chopper - form an integral unit that is designated to rotate about an axis through the center of

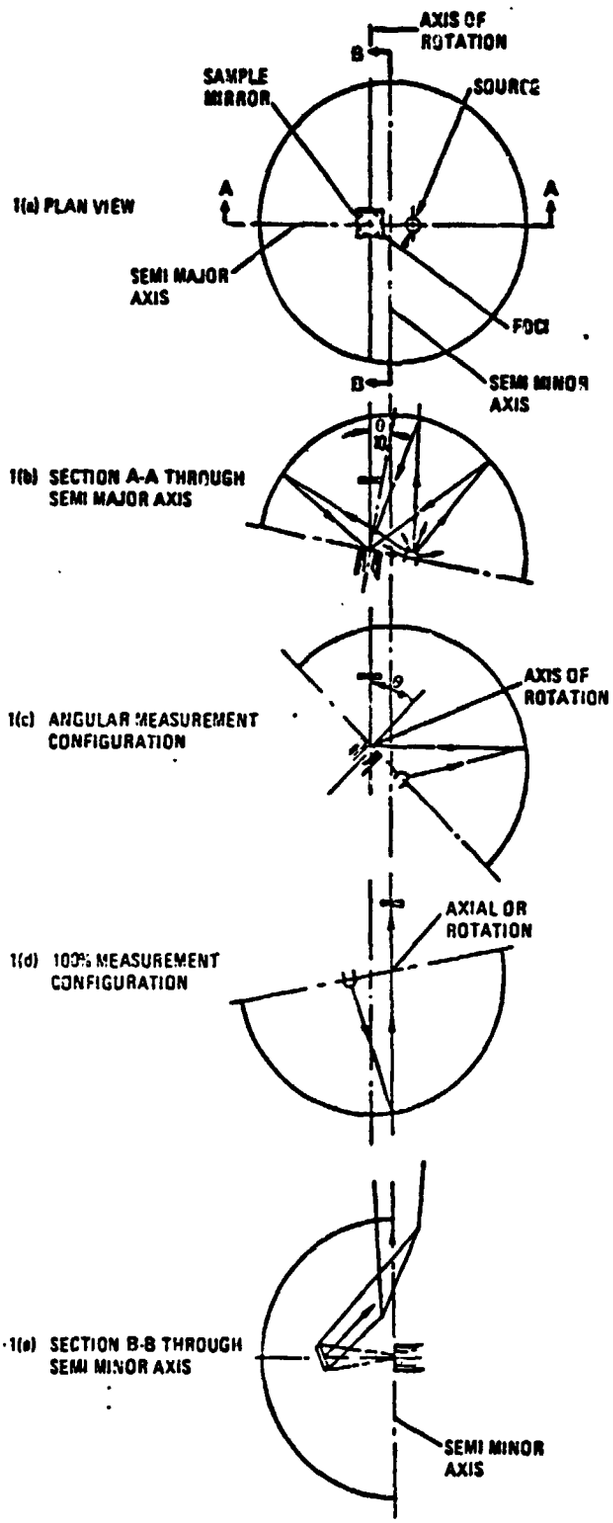

Figure 13. Ellipsometer System

the sample, as shown in Figures 13 and 14. The light gathering and transfer optics, consisting of a small overhead mirror (M1) and subsequent mirrors (M2, M3, and M4), are fixed and do not rotate. Mirrors M1 and M2 are held in position by a bracket that anchors into the central tee, to which the vacuum pump is attached. For making routine near-normal measurements, as required in this work, the ellipse rotation is set as shown in Figure 13. The overhead mirror (M1) views the sample from 10 degrees off normal. To obtain the 100% datum (see Figure 13), the sample is removed from its position at one of the foci and the ellipse is rotated so that the small overhead mirror (M1) receives the full radiation incident on the sample position (but with the sample removed), thus providing a system for true absolute measurements. The data is digitized and computer-processed.

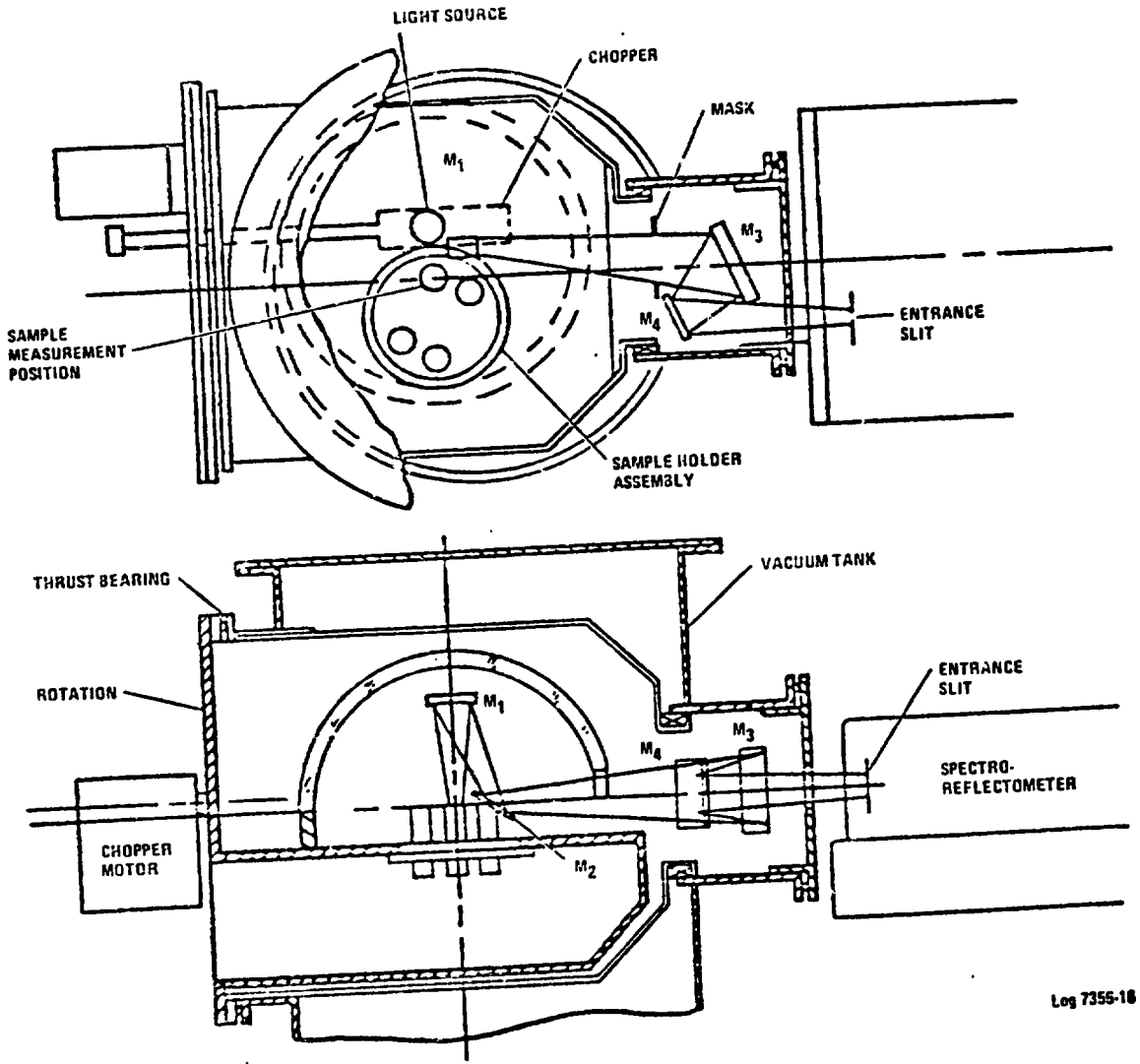

Figure 14. Optical Schematic of Ellipsometer

TEST RESULTS

Thermal Conductivity

Test results for each specimen were plotted against mean specimen temperature and best-fit quadratics drawn through the data. These curves are presented in Figures 15 through 22. Tabular data is contained in the Appendix.

It was expected that both materials would have nearly the same thermal conductivities. The fiber was the same in both cases and the resins were generically the same. As the data indicates, this was the case in the directions where the matrix dominates, i.e., unidirectional Y (Figures 16 and 20) and isotropic Z (Figures 18 and 22).

Conductivity in the unidirectional Y direction was higher than the isotropic Z for both materials (Figures 16 and 18 and Figures 20 and 22). This is the result of fibers in the pre-preg crossing each other and providing higher conduction paths across the ply than those provided by the matrix alone.

Results for the directions where the fiber properties dominate, however, were not similar. Near room temperature, values for the HTS/PMR 15 specimens were higher than the HTS/NR 150B2 specimens by a factor of 2-3 in the unidirectional X (Figures 15 and 19) and isotropic X directions (Figures 17 and 21).

If there were significant differences in fiber properties or effective geometry in these directions, it would be expected to also show as differences in expansion and tensile strength in these directions. Review of that data does not support this. The one significant difference between the materials observed is the high porosity of the HTS/NR 150B2. In the thermal conductivity measurement for these directions, heat is introduced into the end of the specimen through mechanical clamps. Every attempt is made, using conductive coatings and special clamps, to obtain good thermal contact. However, only the specimen outer surfaces are contacted. Little, if any, direct contact to fibers is made. Heat must be carried through some matrix before entering the fibers which are the primary conductors.

Normally, thermal gradients through the specimen become small a short distance from the ends which means that heat flow is mostly longitudinal and that most fibers are equally involved. High porosity, however, could change this. If these short paths from the heat source to the fibers are through voids rather than matrix then fibers down from the surface may have little contribution to the total heat flow making the conductivity look low. However, voids in the matrix should also affect the unidirectional Y and isotropic Z conductivity but, in this case, they appear not to have.

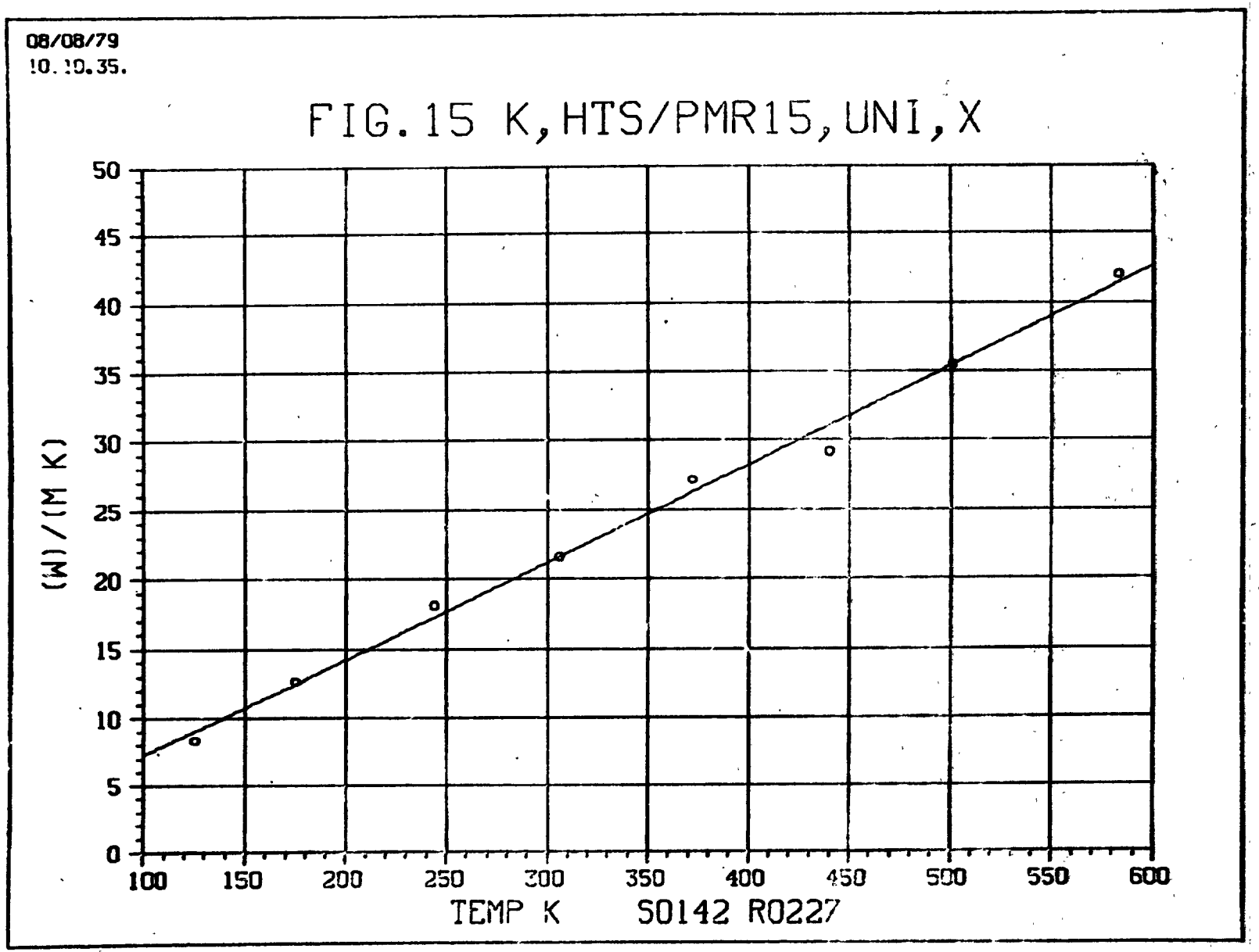
08/08/79
10.10.35.
FIG. 15 K, HTS/PMR15, UNI, X
(W) / (M K)
50
45
40
35
30
25
20
15
10
5
0
100
150
200
250
300
350
400
450
500
550
600
TEMP K
S0142 R0227

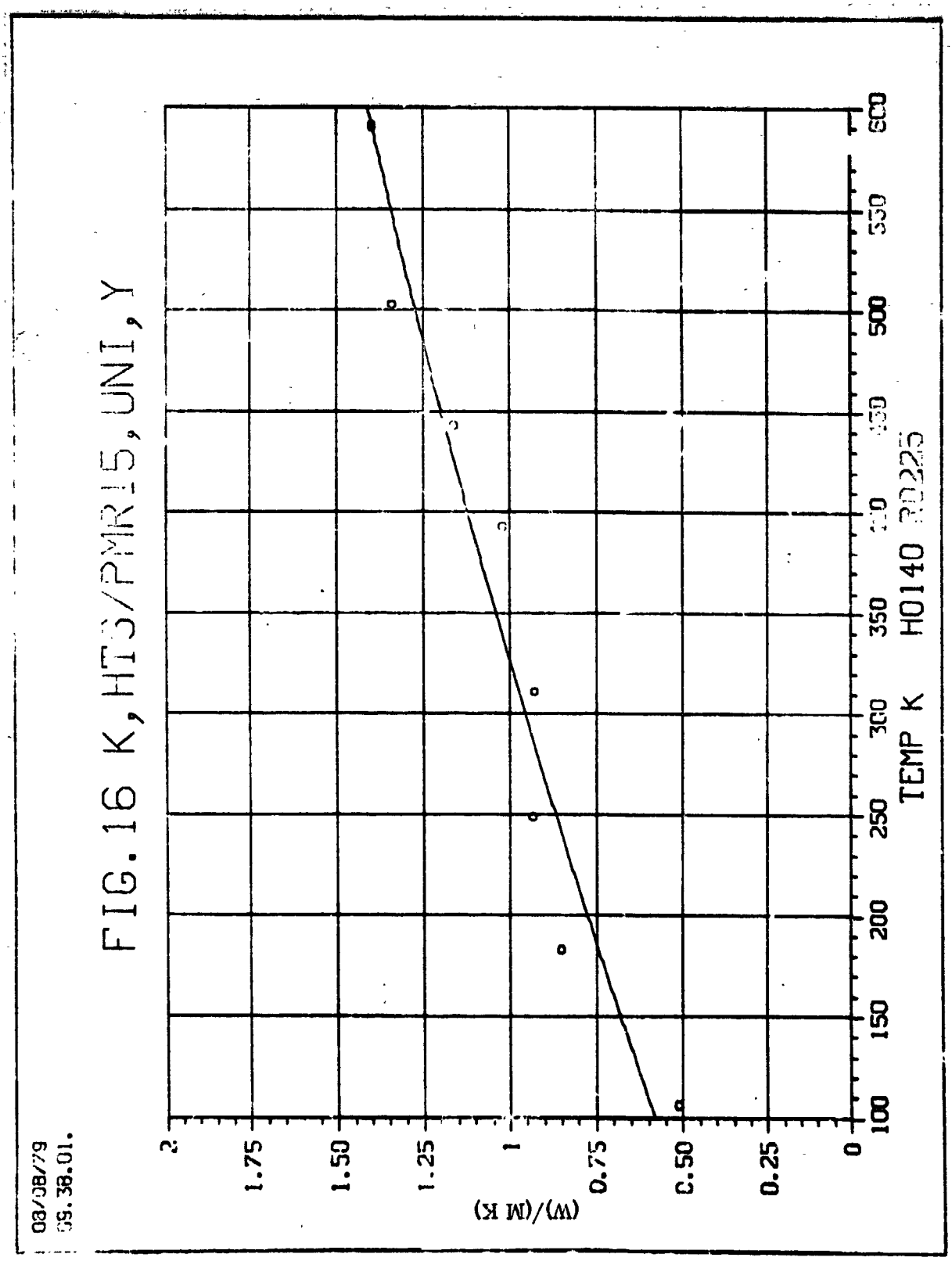

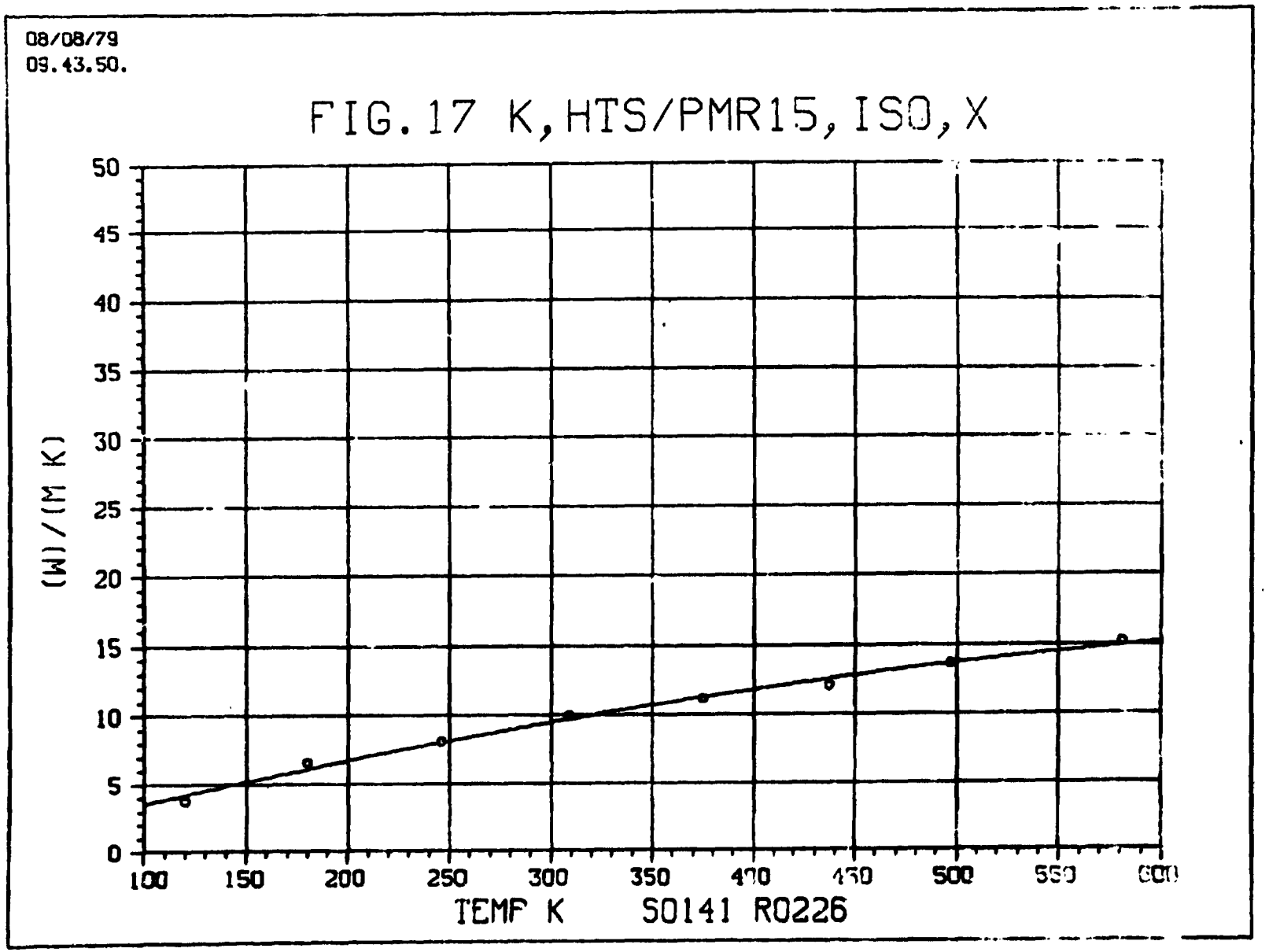
08/08/79
09.43.50.
FIG. 17 K, HTS/PMR15, ISO, X
(W)/(M K)
50
45
40
35
30
25
20
15
10
5
0
100
150
200
250
300
350
400
450
500
550
600
TEMP K
S0141 R0226

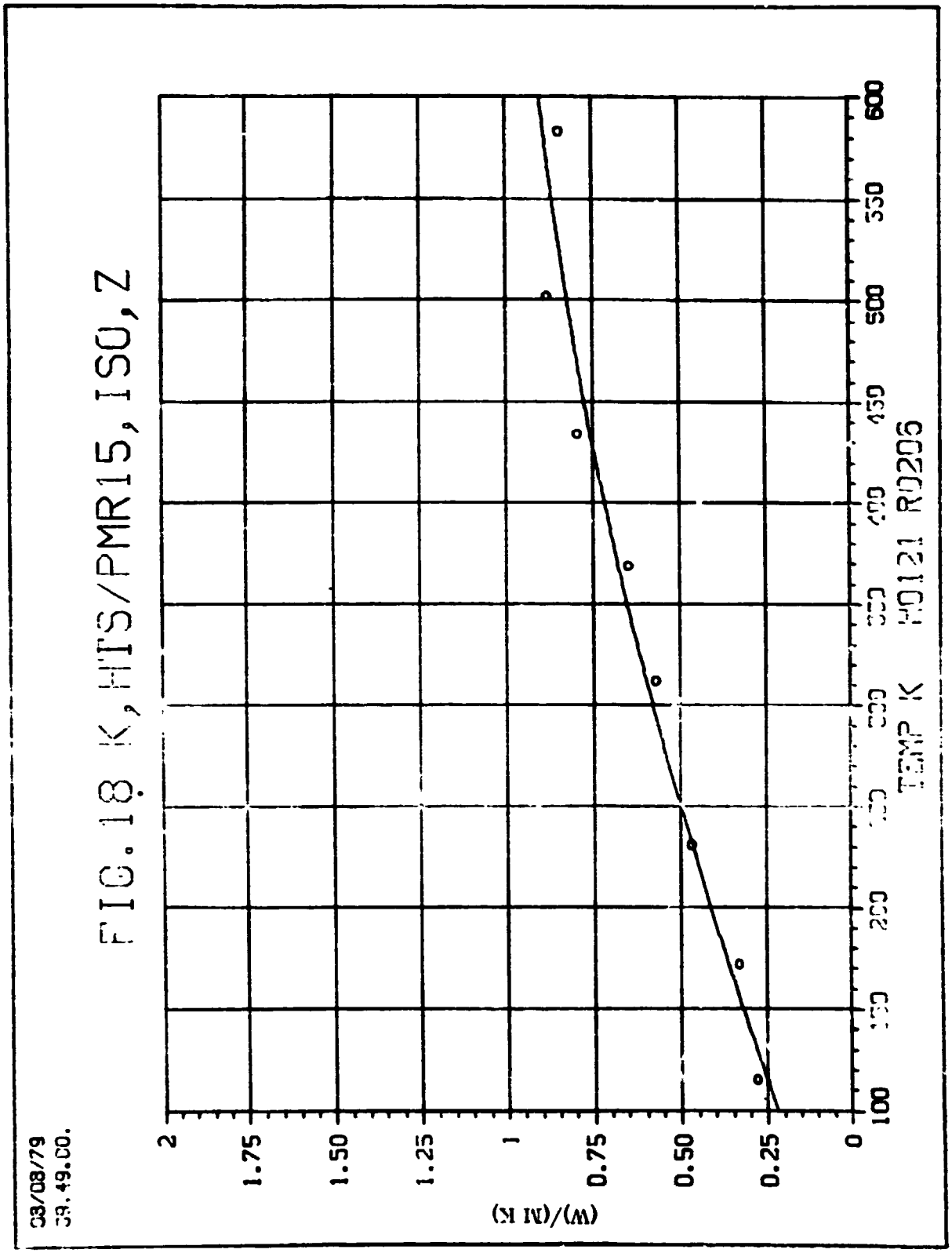

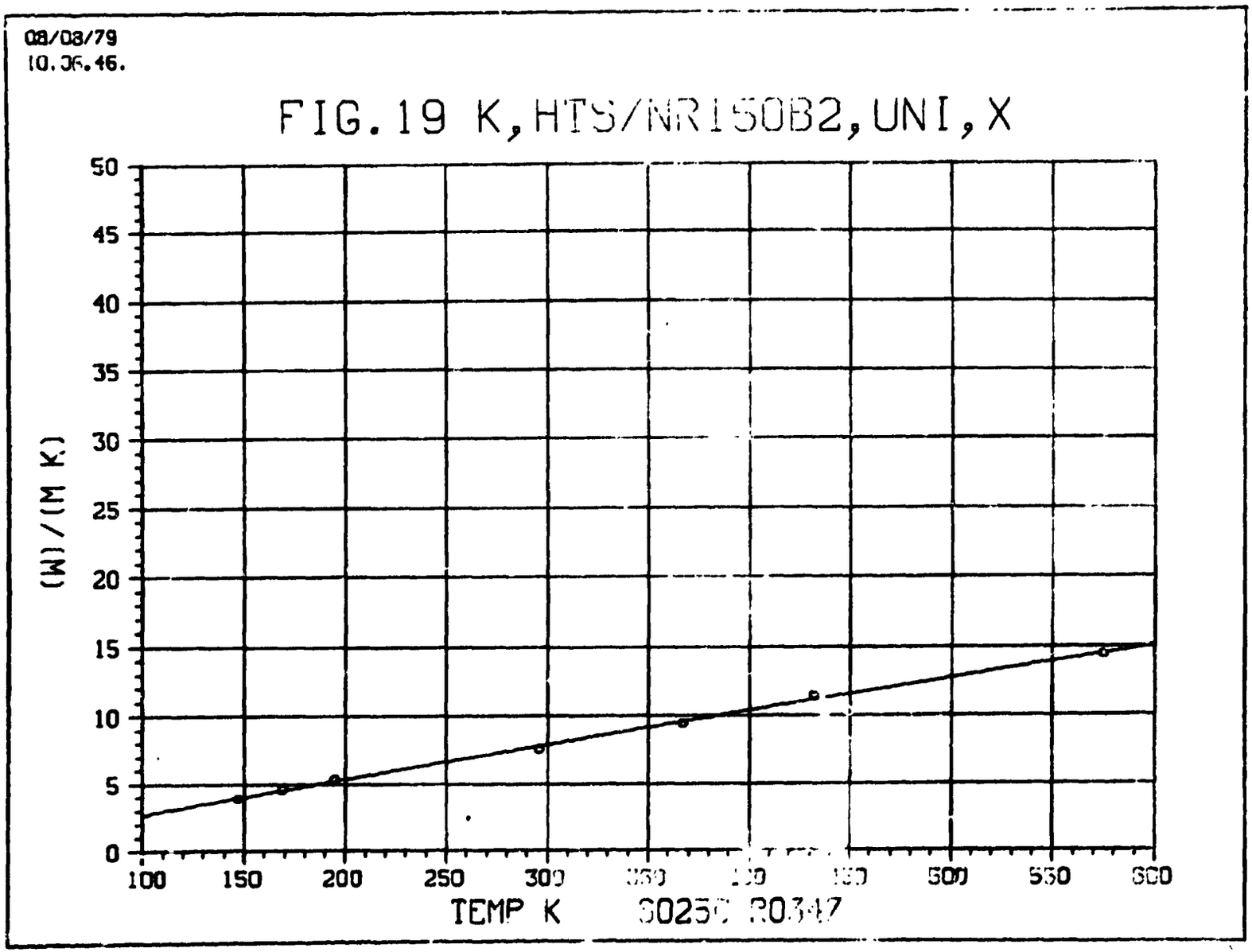
08/08/79
10.36.46.
FIG. 19 K, HTS/NR150B2, UNI, X
(W) / (M K)
50
45
40
35
30
25
20
15
10
5
0
100
150
200
250
300
500
550
600
TEMP K

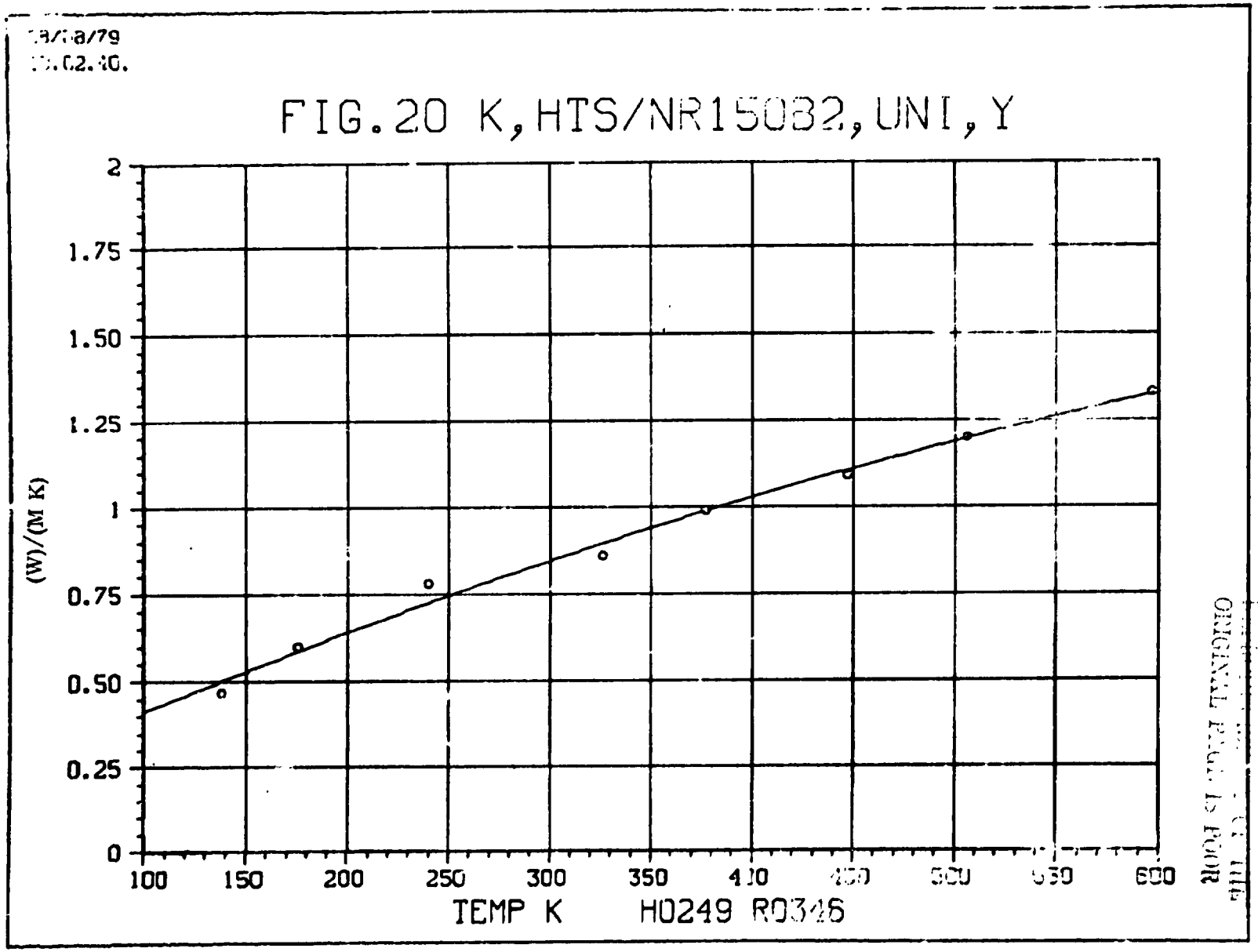
FIG.20 K,HTS/NR15082,UNI,Y
(W)/(M K)
2
1.75
1.50
1.25
1
0.75
0.50
0.25
0
100
150
200
250
300
350
400
450
500
550
600
TEMP K
H0249 R0346

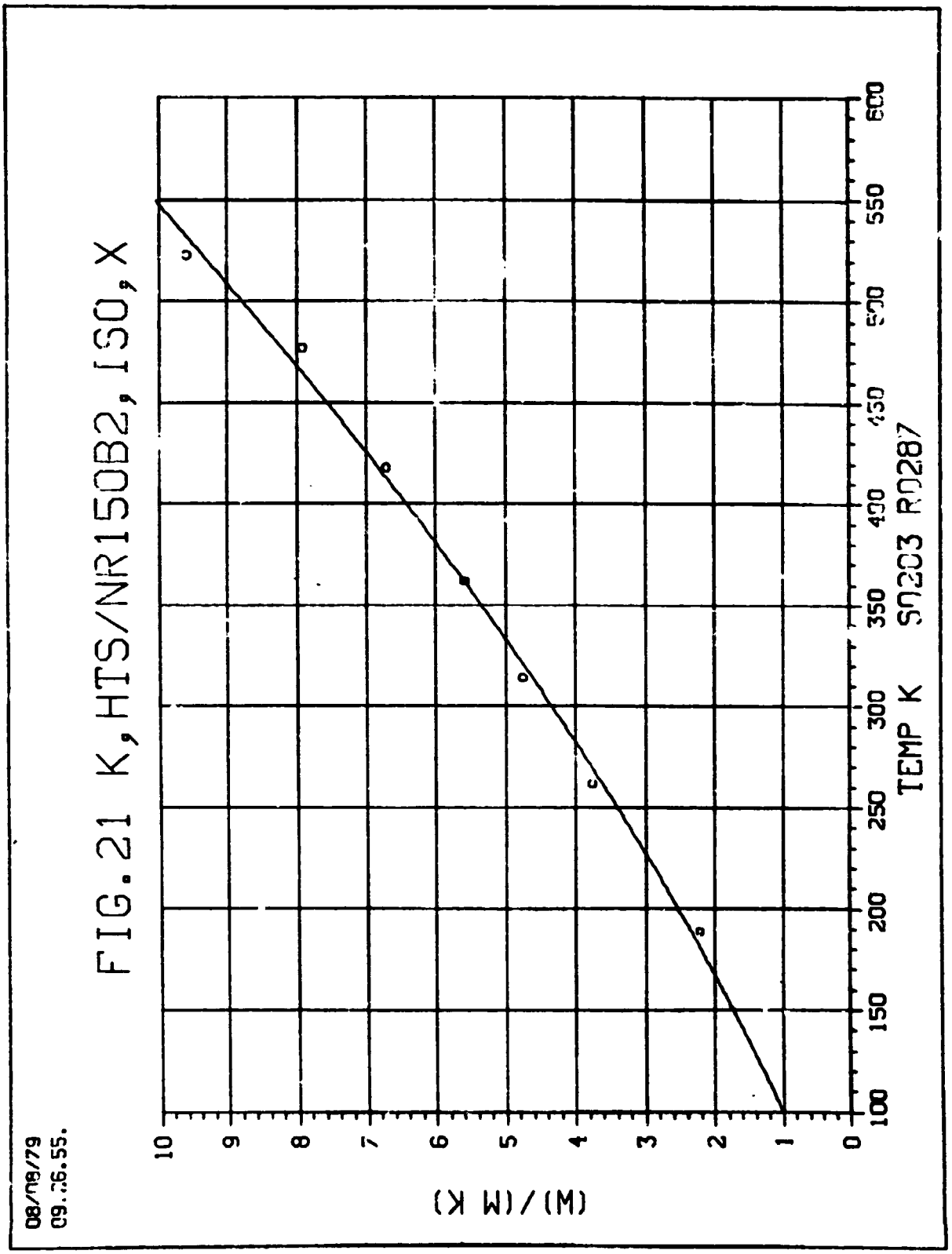
FIG.21 K,HTS/NR150B2, ISO, X
08/08/79
09.36.55.
(K M)/(M)
10
9
8
7
6
5
4
3
2
1
0
100
150
200
250
300
350
400
450
500
550
600
TEMP K
S0203 R0287

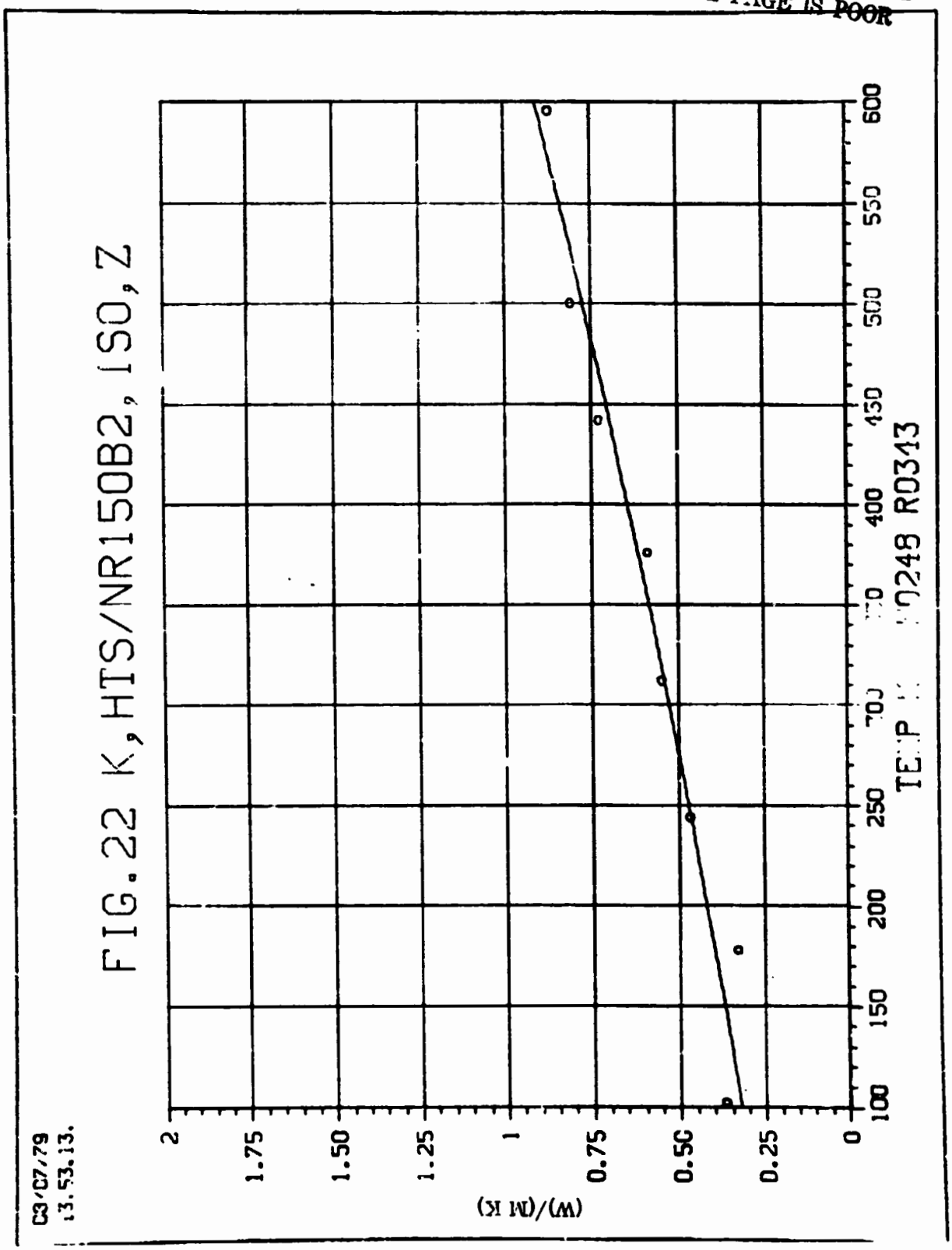

It is speculated that the voids are not sufficient to reduce the conduction through the matrix significantly but do result in poor contact between fiber and matrix.

Thermal Expansion

As a graphite fiber-reinforced organic matrix composite is heated, the negative coefficient of thermal expansion (CTE) fiber tries to contract while the positive CTE matrix tries to expand. The resulting length of the composite is dependent on many factors which include:

- fiber and matrix CTE
- fiber and matrix modulus
- fiber and matrix percentages
- voids and impurities
- fiber orientation
- residual stresses
- fiber-matrix interface

The above list is far from complete but includes those factors which produce the significant effects. Most of the above are subject to variations from laminate to laminate and from point to point within a laminate. Some can change as the laminate is exposed to various environments including the expansion measurement itself.

As the temperature of such a composite is varied, variations in one or more significant parameters result in changes in the rate of length change with temperature. Thus, CTE's ($\Delta l / l$/degree) are not constant. In fact, they may not even vary smoothly. For this reason, it is not appropriate to quote a value for the CTE of a composite except when referring to a narrow, specific temperature range.

It is more appropriate to present data graphically in the form of $\Delta l / l$ versus temperature so that the thermal strain from point to point can be seen. All expansion data obtained on this program is presented in this form in Figures 23 through 38. The lines connecting the individual Δl points are straight lines and do not necessarily represent specimen behavior between the discreet points. Tabular data is contained in the Appendix.

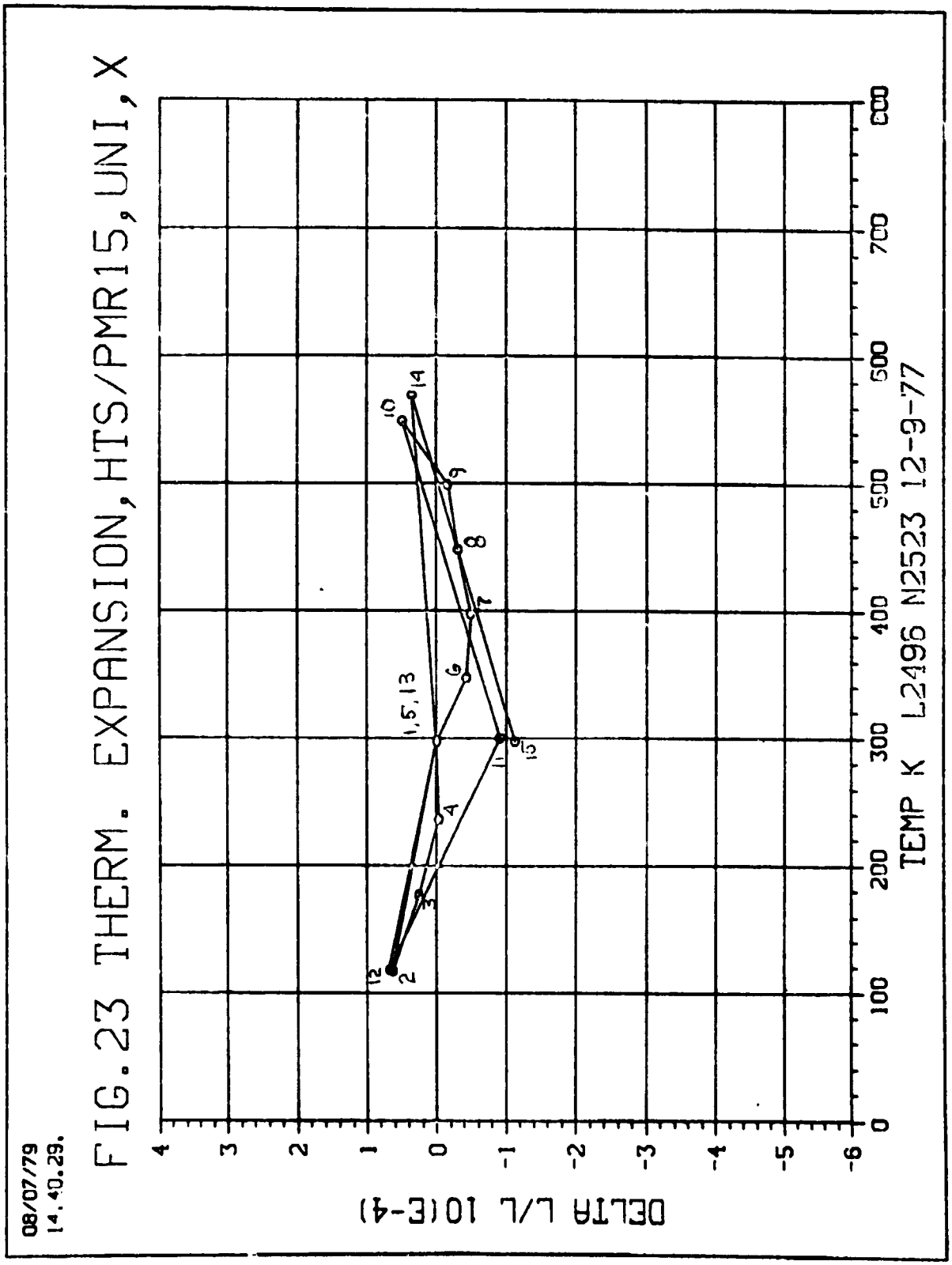

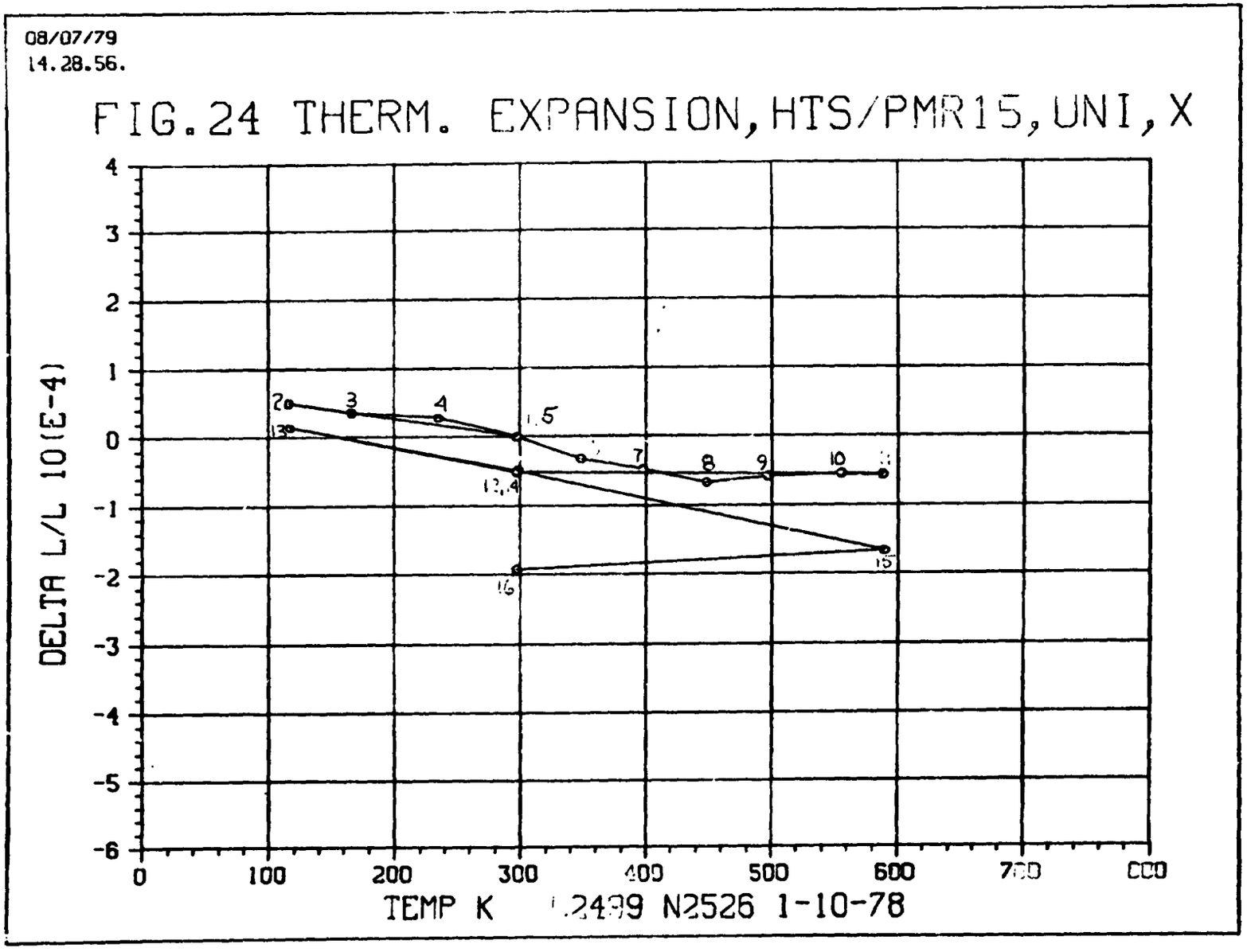
08/07/79
14.28.56.
FIG.24 THERM. EXPANSION,HTS/PMR15,UNI,X
DELTA L/L 10(E-4)
TEMP K
2499 N2526 1-10-78

10/03/73
09.18.30.

FIG. 25 THERM. EXPANSION, HTS/NR150B2, UNI, X

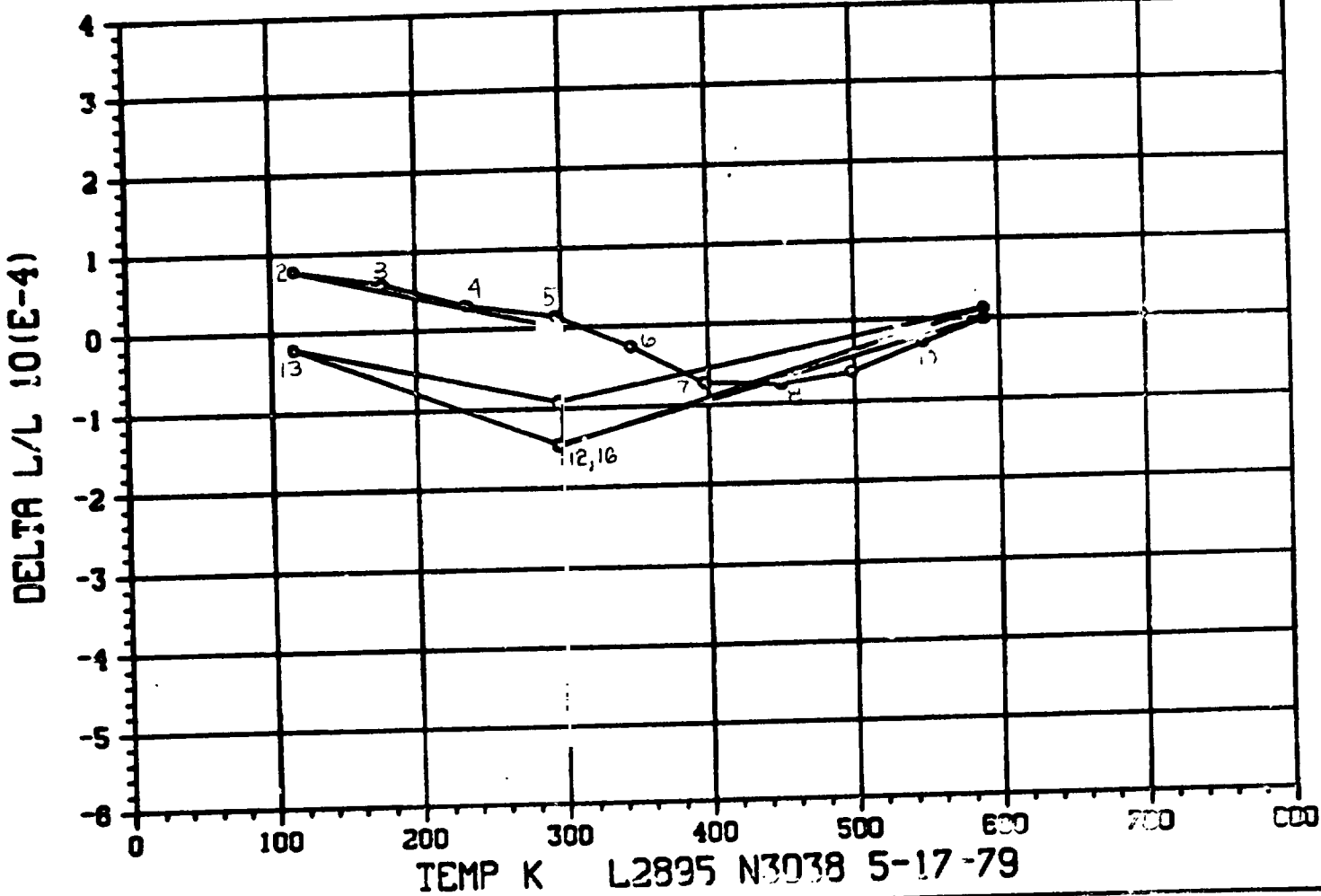

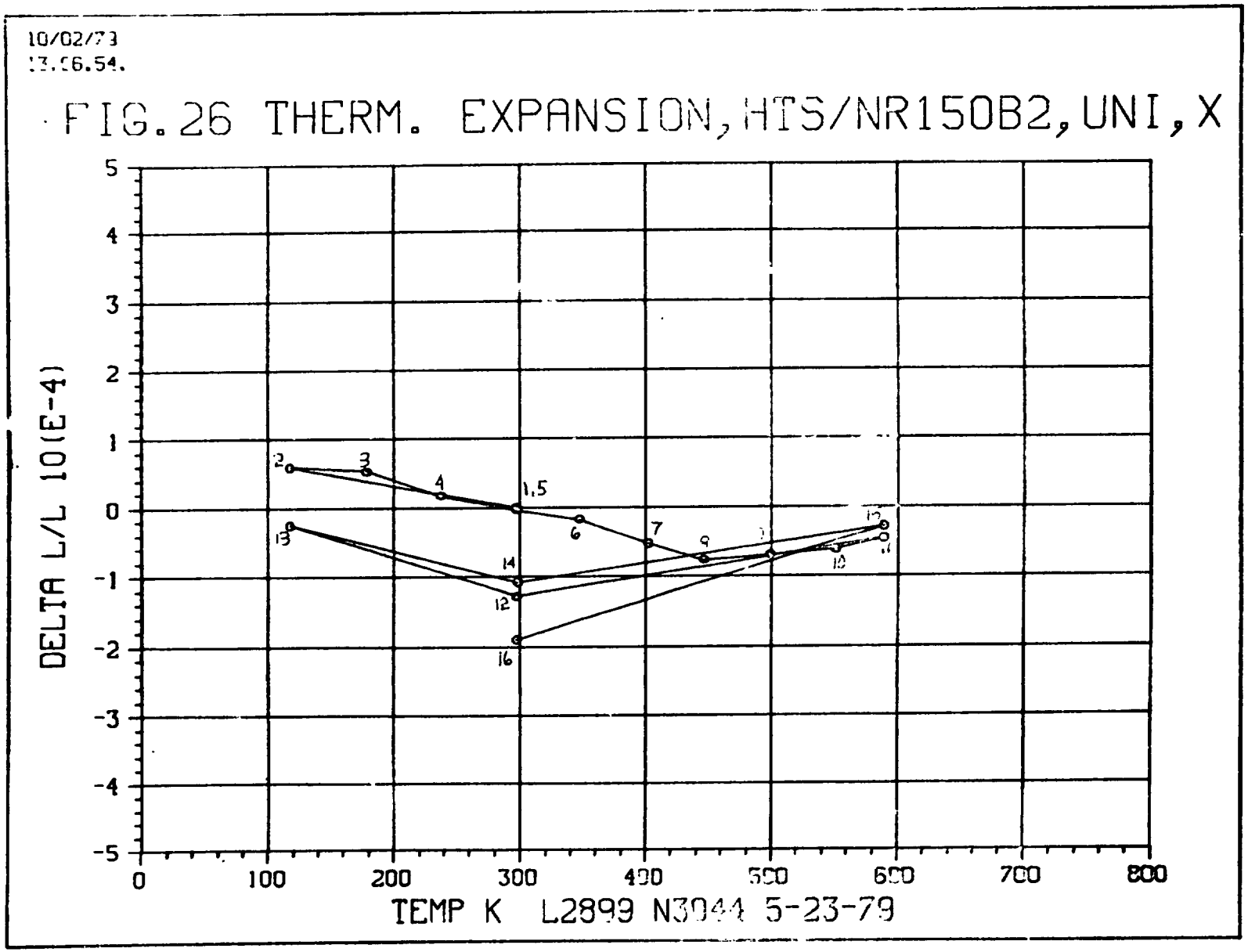
10/02/73
13.06.54.
FIG.26 THERM. EXPANSION,HTS/NR150B2,UNI,X
DELTA L/L 10(E-4)
5
4
3
2
1
0
-1
-2
-3
-4
-5
0
100
200
300
400
500
600
700
800
TEMP K L2899 N3044 5-23-79
2
3
4
1,5
6
7
9
13
14
12
16
18

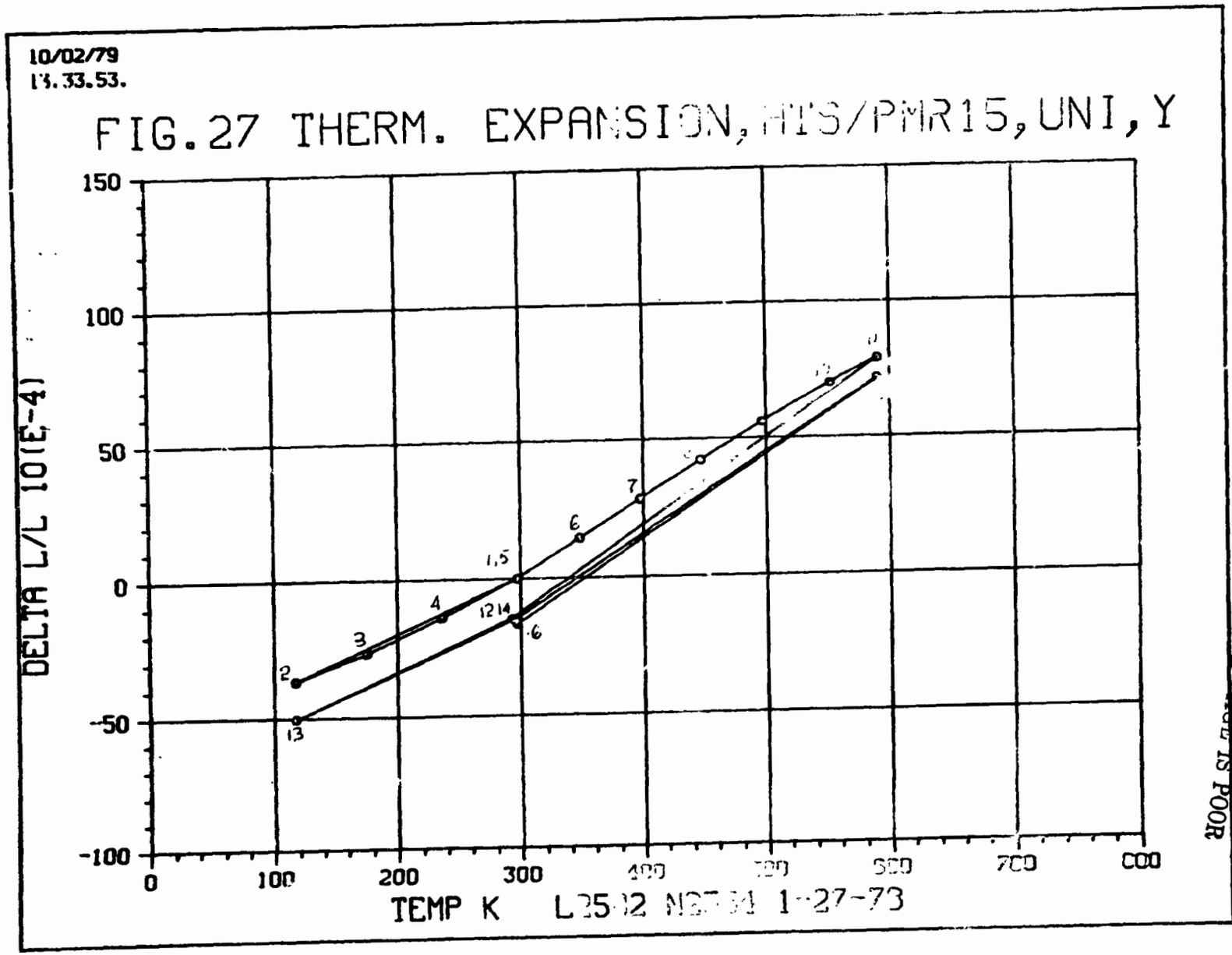

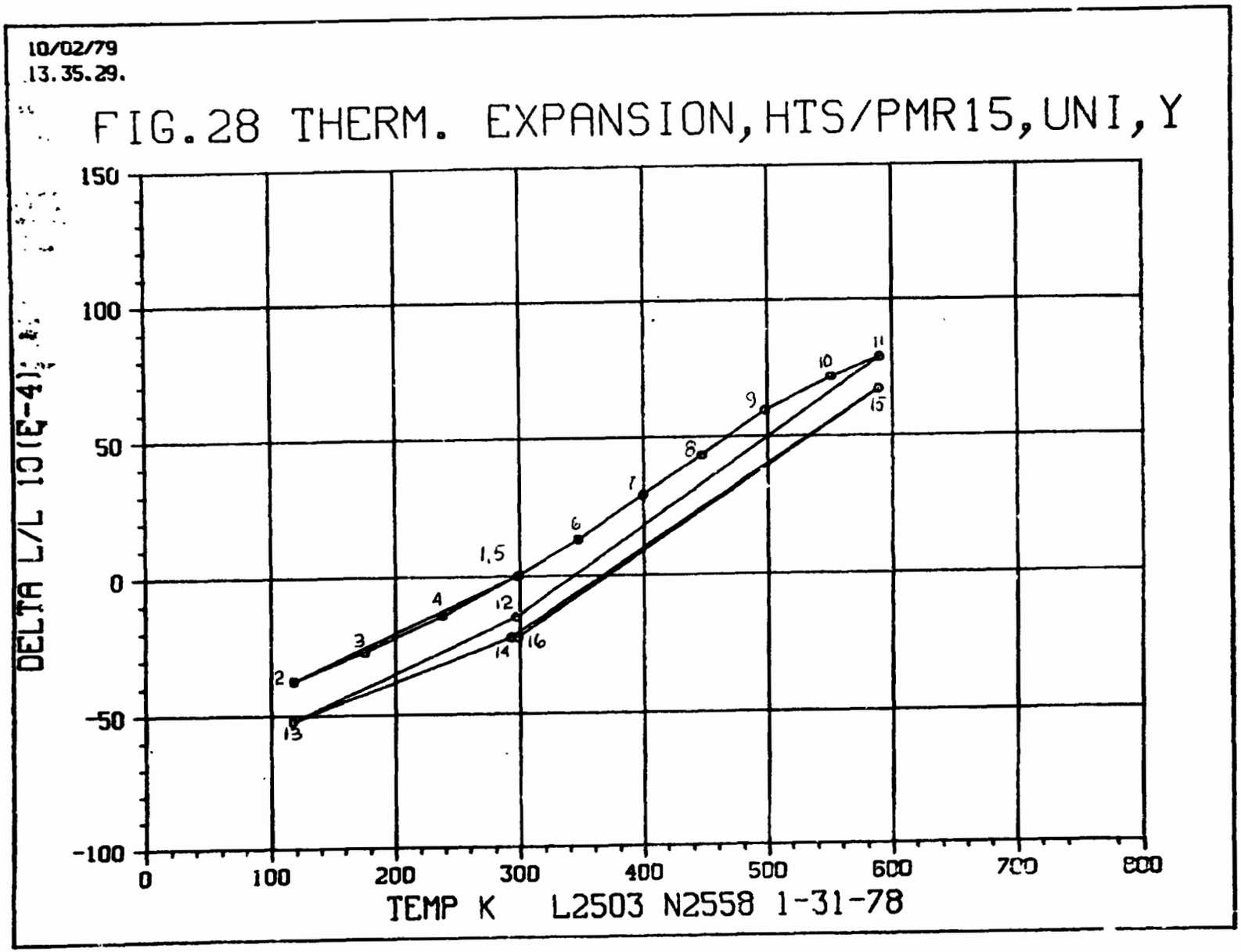
10/02/79
13.35.29.
FIG.28 THERM. EXPANSION,HTS/PMR15,UNI,Y
DELTA L/L 10(E-4)
150
100
50
0
-50
-100
0
100
200
300
400
500
600
700
800
TEMP K L2503 N2558 1-31-78
1,5
2
3
4
6
7
8
9
10
11
12
13
14
15
16

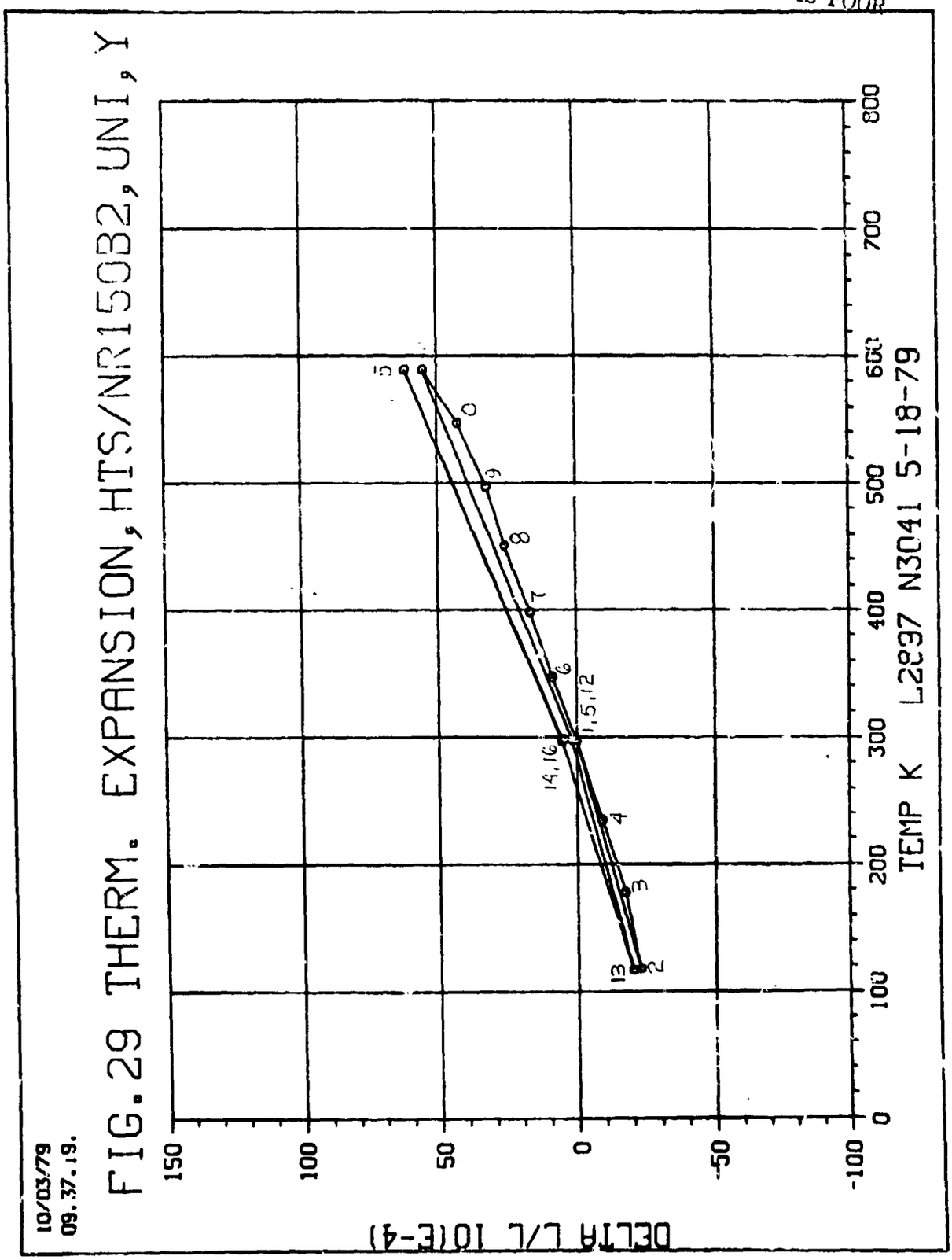

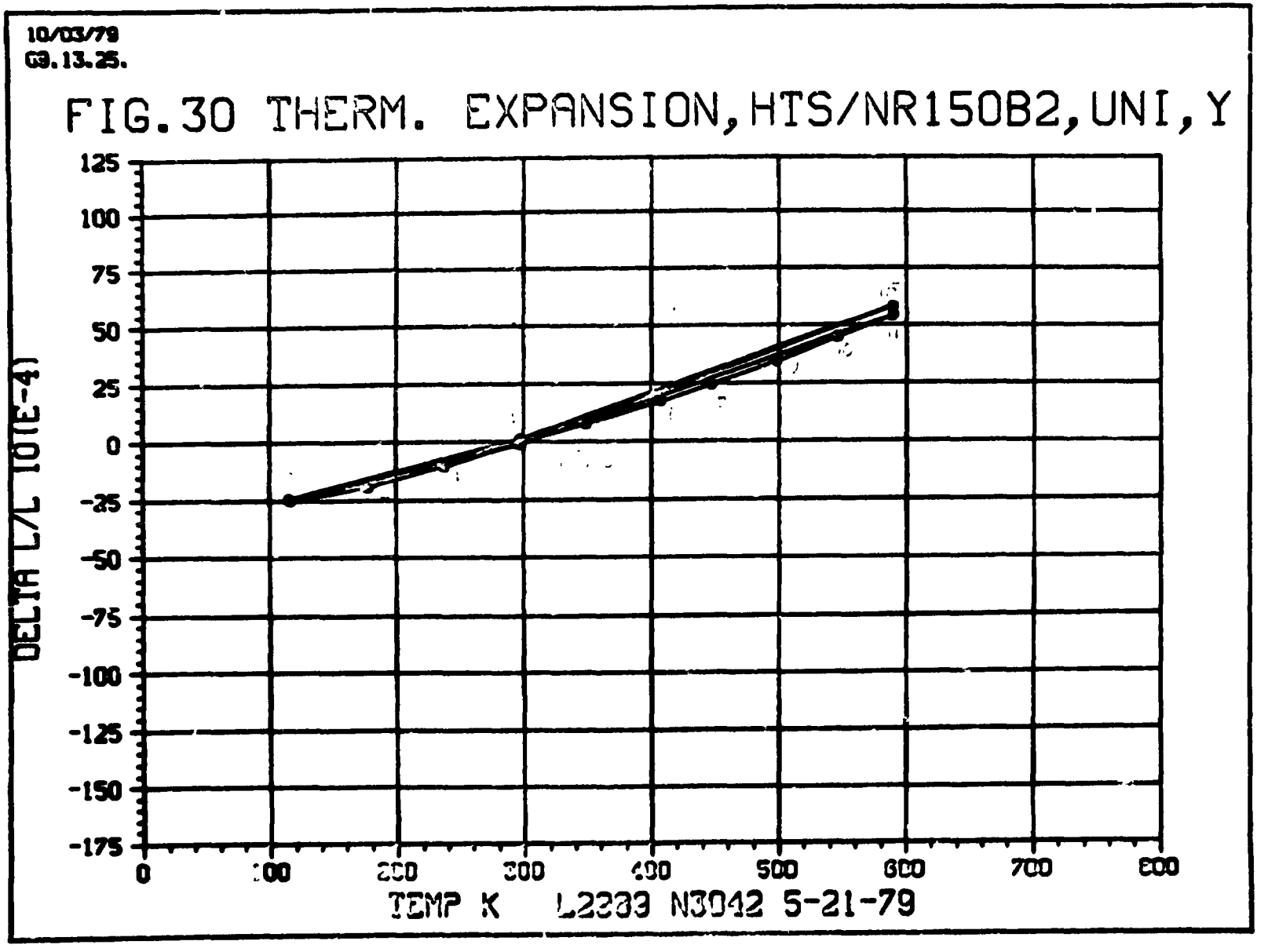
10/03/79
09.13.25.
FIG.30 THERM. EXPANSION,HTS/NR150B2,UNI,Y
DELTA L/L 10(E-4)
125
100
75
50
25
0
-25
-50
-75
-100
-125
-150
-175
0
100
200
300
400
500
600
700
800
TEMP K L2333 N3042 5-21-79

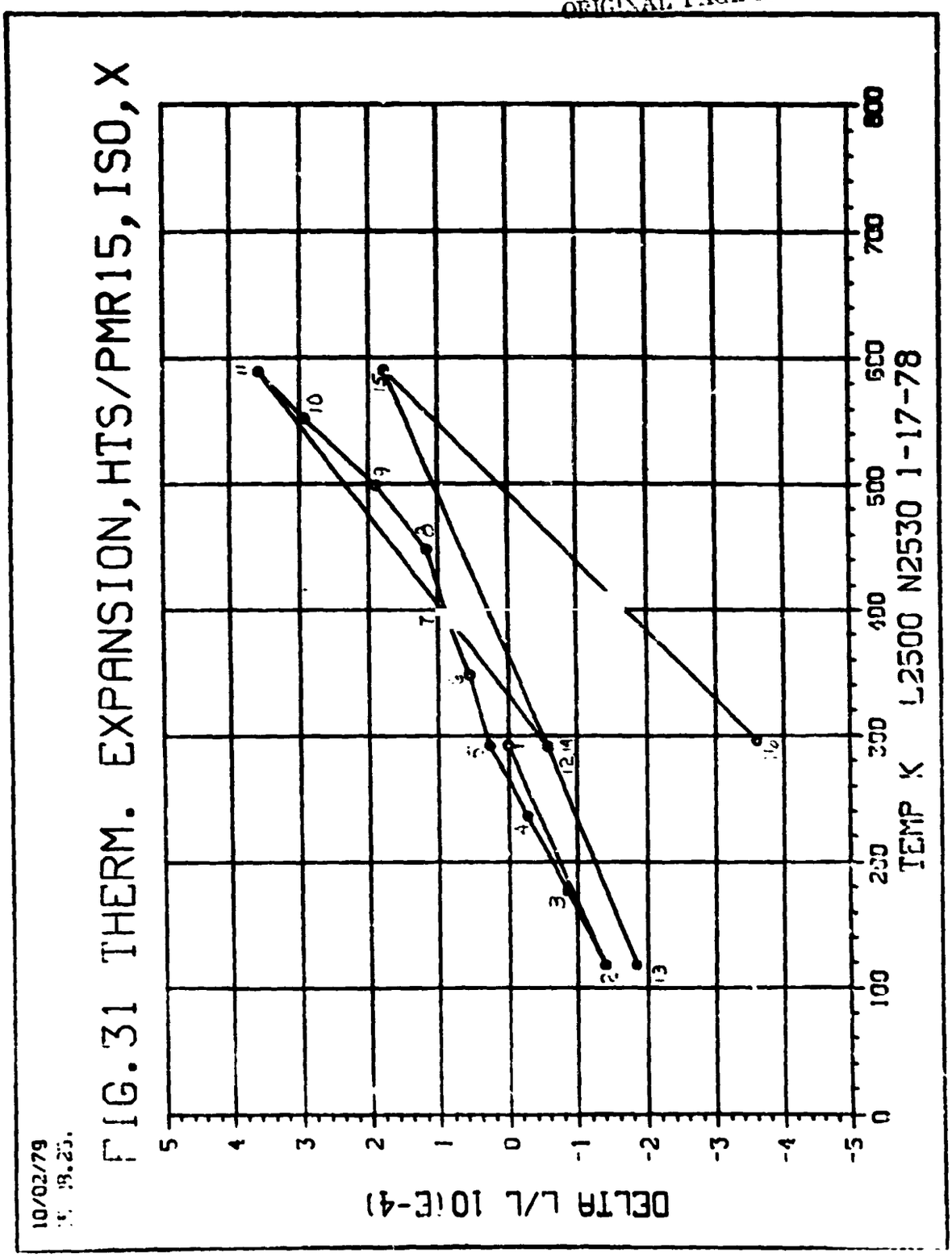

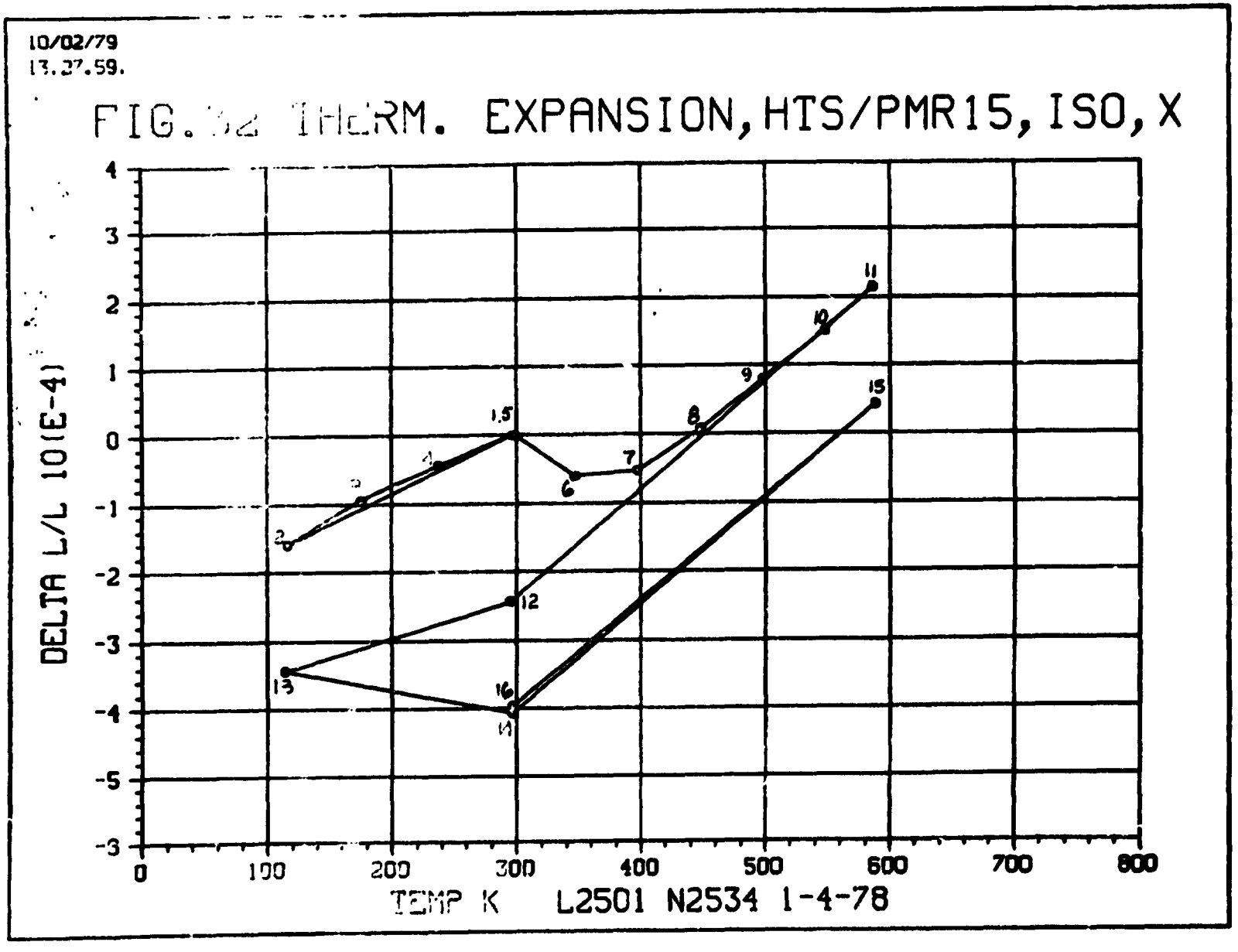
10/02/79
13.27.59.
FIG. 52 THERM. EXPANSION, HTS/PMR15, ISO, X
DELTA L/L 10(E-4)
4
3
2
1
0
-1
-2
-3
-4
-5
-3
0
100
200
300
400
500
600
700
800
TEMP K
L2501 N2534 1-4-78
1
2
3
4
5
6
7
8
9
10
11
12
13
14
15
16

For comparison purposes, CTE values typical of the results for each specimen are given in Table 3. Since the results often varied from cycle to cycle, they are only representative values to indicate the gross behavior of the sample. Where there were significant differences between slopes above and below ambient temperature two values are listed.

Unidirectional

The combination of the negative CTE fiber and the positive CTE resin produced very low expansion in the X direction of both unidirectional layups. Here, the full effect of the fibers is exhibited. During the initial thermal cycle both materials had slope sign changes from minus to plus in the 400 - 450 K range. Slopes ranged from approximately $-.4 \times 10^{-6}$ m/m/K to $+.6 \times 10^{-6}$ m/m/K for the PMR 15 specimens and from $-.5 \times 10^{-6}$ m/m/K to $-.5 \times 10^{-6}$ m/m/K for the NR 150 specimens.

Both materials showed a tendency to not return to the original length on successive thermal cycles. Differences between values at 300K were as great as 2×10^{-4} m/m for the NR 150 specimens (Figures 25 and 26). With the exception of the final cycle on L2409, this scatter was roughly half for the PMR 15 specimens (Figures 23 and 24).

The first 11 points of each run (one full cycle) were taken to define details of the behavior of the specimen over the full temperature range. The remaining points were taken to assess the reproducibility of the behavior between end points. Points were taken only at ambient (300K) and the extremes. The rate of temperature change between these points was considerably higher than for the first 11 points because a greater range was covered in approximately the same time. It is not uncommon for fiber reinforced composites to behave differently as the cycling rate varies, particularly in the directions where the CTE is close to zero.

In the Y direction of the unidirectional laminates where the matrix CTE dominates, the matrix differences are evident (Figures 27-30). CTE's were approximately 24×10^{-6} m/m/K for the PMR 15 specimens and 16×10^{-6} m/m/K for the NR 150. These differences did not show in the X direction where the common fiber dominates.

Scatter in the Δl data for the PMR 15 specimens was nearly twice as great as for the NR 150 specimens.

Quasi-isotropic

With fewer fibers oriented in the X direction the CTE in the X direction of a quasi-isotropic laminate should be more positive than the X direction of a unidirectional laminate for the same graphite fiber and matrix. This was, indeed, the case for both

Table 3. Representative Expansion Coefficients

Material	Layup	Direction	Specimen	Representative Coefficient (10^{-6} m/m/K) Low End/High End
HTS/PMR15	Uni	X	L2499	-.2/0
			L2496	-.4/.6
HTS/NR150B2	Uni	X	L2895	-.5/.5
			L2899	-.4/.2
HTS/PMR15	Uni	Y	L2502	24.
			L2503	24.
HTS/NR150B2	Uni	Y	L2897	16.
			L2898	16.
HTS/PMR15	Iso	X	L2500	.8/1.7
			L2501	.8/1.5
HTS/NR150B2	Iso	X	L2894	.3/1.
			L2893	.4/1.2
HTS/PMR15	Iso	Z	L2504	30.
			L2548	-4/20
HTS/NR150B2	Iso	Z	L2928	17.
			L2929	23.

materials with the CTE tending to be positive over most of the temperature range rather than negative at the low end and slightly positive at the high end for the unidirectional layups (Figures 23-26 and 31-34).

Expansion of the PMR 15 specimens was considerably greater than that of the NR 150B2 specimens with the former yielding slopes in the order of .8 to 1.7 x 10^{-6} m/m/K and the latter .3 to 1.2 x 10^{-6} m/m/K.

Both materials exhibited a large amount of scatter over the thermal cycles. Differences in ambient lengths were approximately 2 x 10^{-4} m/m for the NR 150B2 and 4 x 10^{-4} m/m for the PMR 15. Both NR 150B2 specimens produced about the same results. Results for the two PMR 15 specimens were different from each other both in shapes of the $\Delta l/l$ curves and total change in length from 113K to 588K.

It is generally assumed that the Z direction in any laminate is similar in CTE to the Y direction in the unidirectional laminate since no fibers run in either of these directions. In reality, the lack of perfect alignment of the fibers in the prepreg creates some fiber effectiveness in the unidirectional Y direction and a lower CTE. This was the case for both materials, with the exception of the very low values for one HTS/PMR 15 isotropic Z specimen, L2548 (Figures 35-38).

Microscopic examination of this specimen revealed it was delaminated in some areas, had excessively non-parallel plies and high void content. The latter two defects would tend to minimize the contribution of the matrix and hence, lower the CTE.

Specific Heat

Specific heat results for both materials are plotted in Figures 39 and 40. The curves are best fit quadratics. The individual data points are tabulated in the Appendix.

Although the fiber is the same in both materials (HTS), the resins are sufficiently different in structure to result in a difference in their specific heats. As the data shows, average specific heat of the PMR 15 samples was consistently higher than that for the NR150 B2.

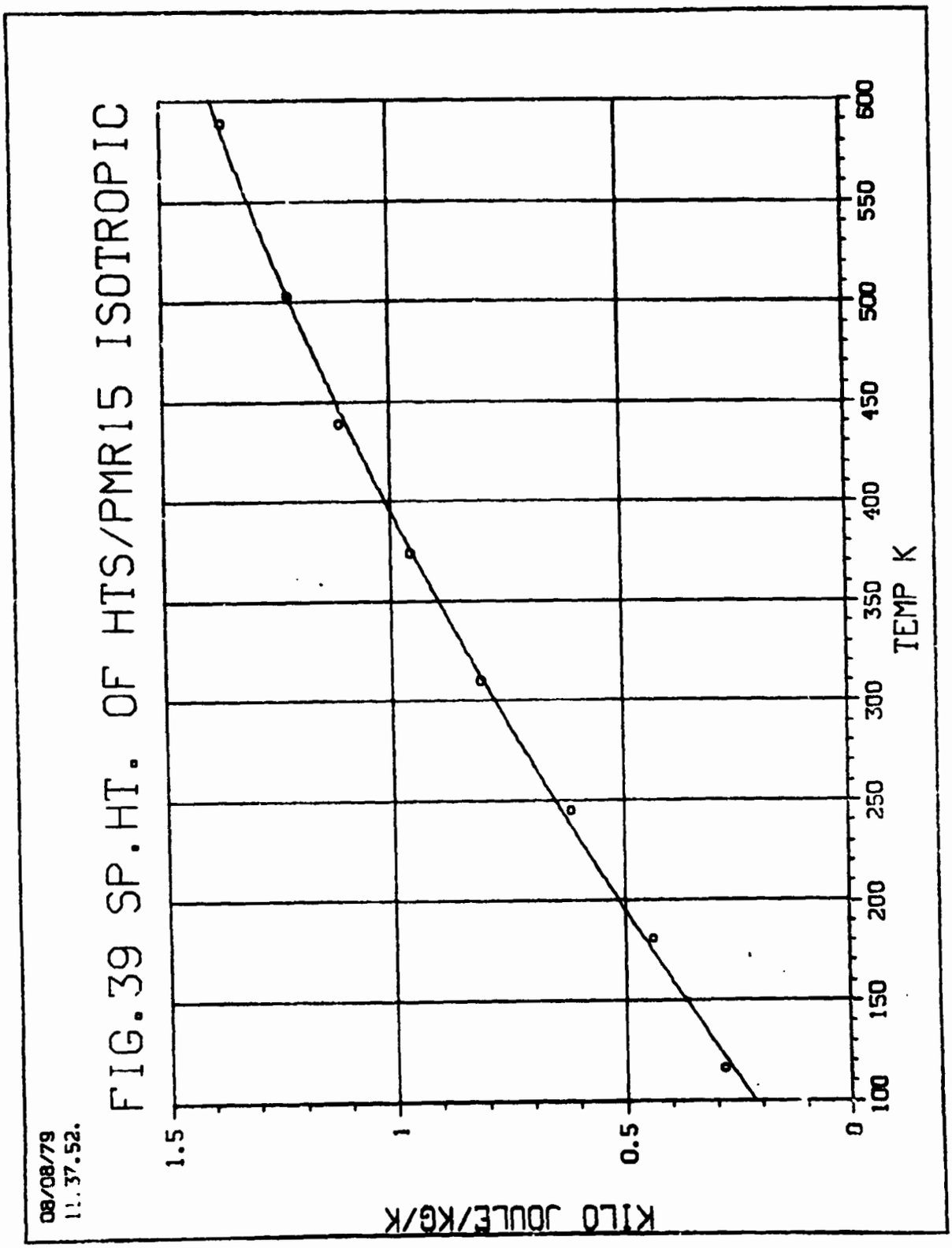
FIG.39 SP.HT. OF HTS/PMR15 ISOTROPIC
08/08/79
11.37.52.
KILO JOULE/KG/K
1.5
1
0.5
0
100
150
200
250
300
350
400
450
500
550
600
TEMP K

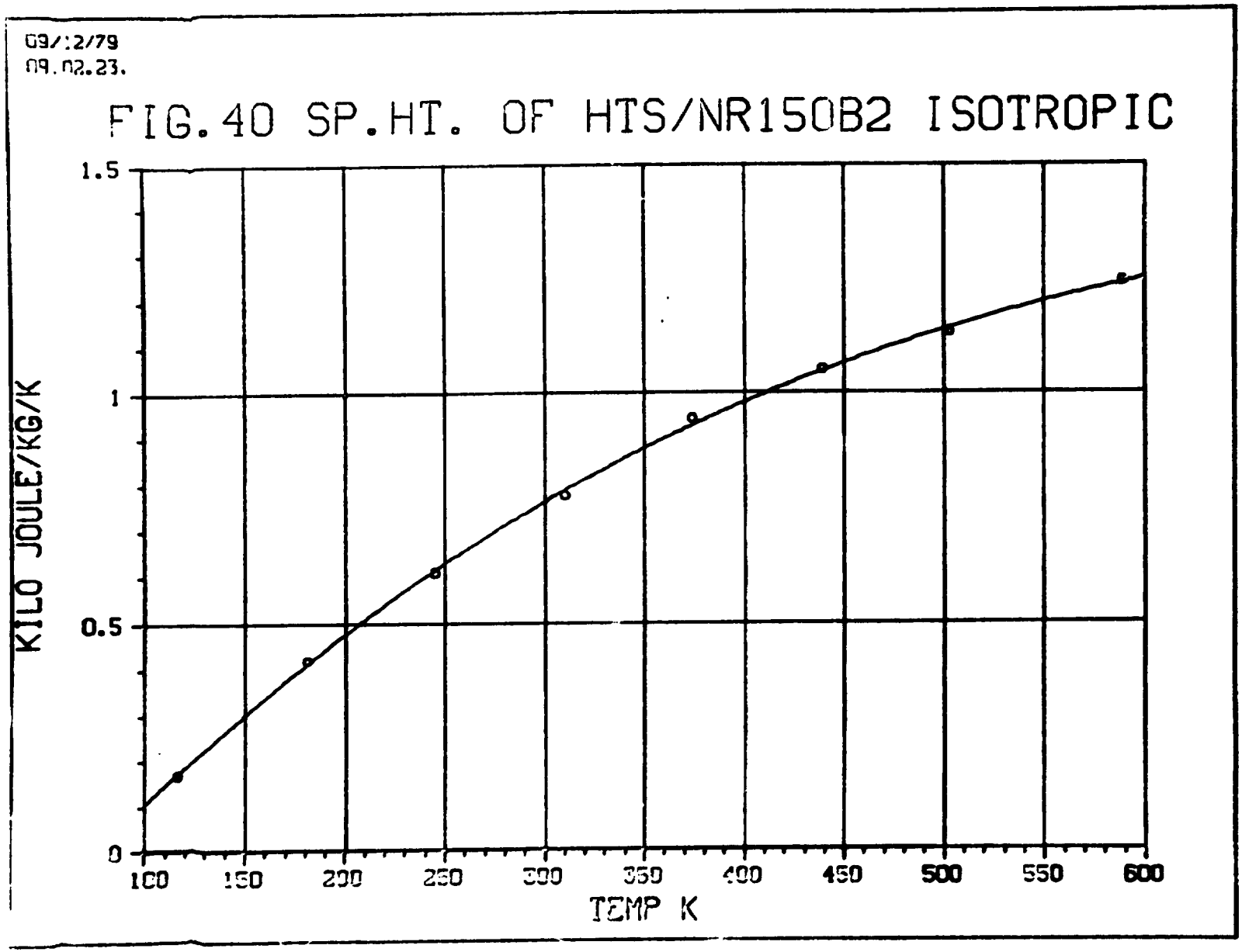
09/12/79
09.02.23.
FIG.40 SP.HT. OF HTS/NR150B2 ISOTROPIC
KILO JOULE/KG/K
1.5
1
0.5
0
100
150
200
250
300
350
400
450
500
550
600
TEMP K

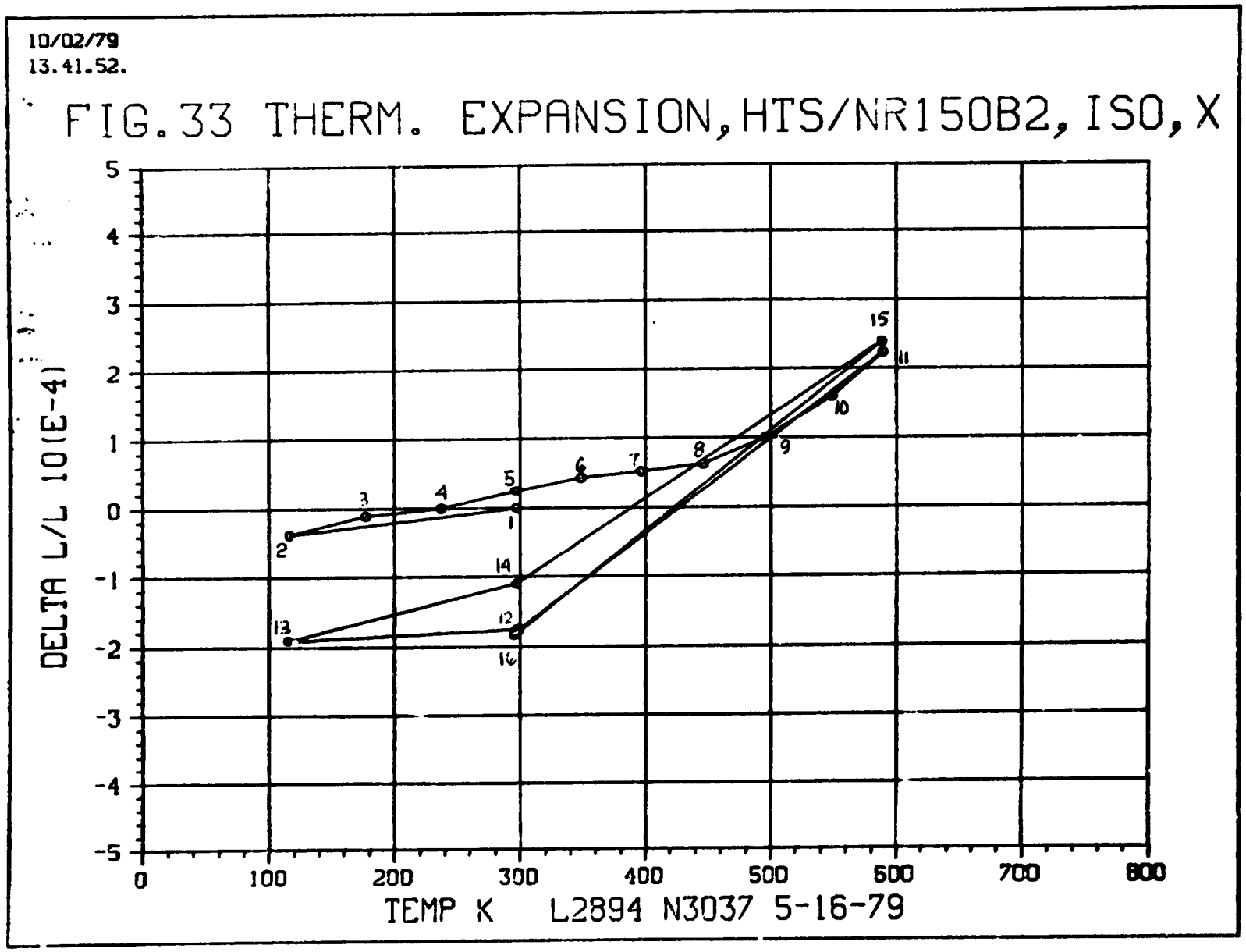
10/02/79
13.41.52.
FIG.33 THERM. EXPANSION, HTS/NR150B2, ISO, X
DELTA L/L 10(E-4)
5
4
3
2
1
0
-1
-2
-3
-4
-5
0
100
200
300
400
500
600
700
800
TEMP K
L2894 N3037 5-16-79
1
2
3
4
5
6
7
8
9
10
11
12
13
14
15
16

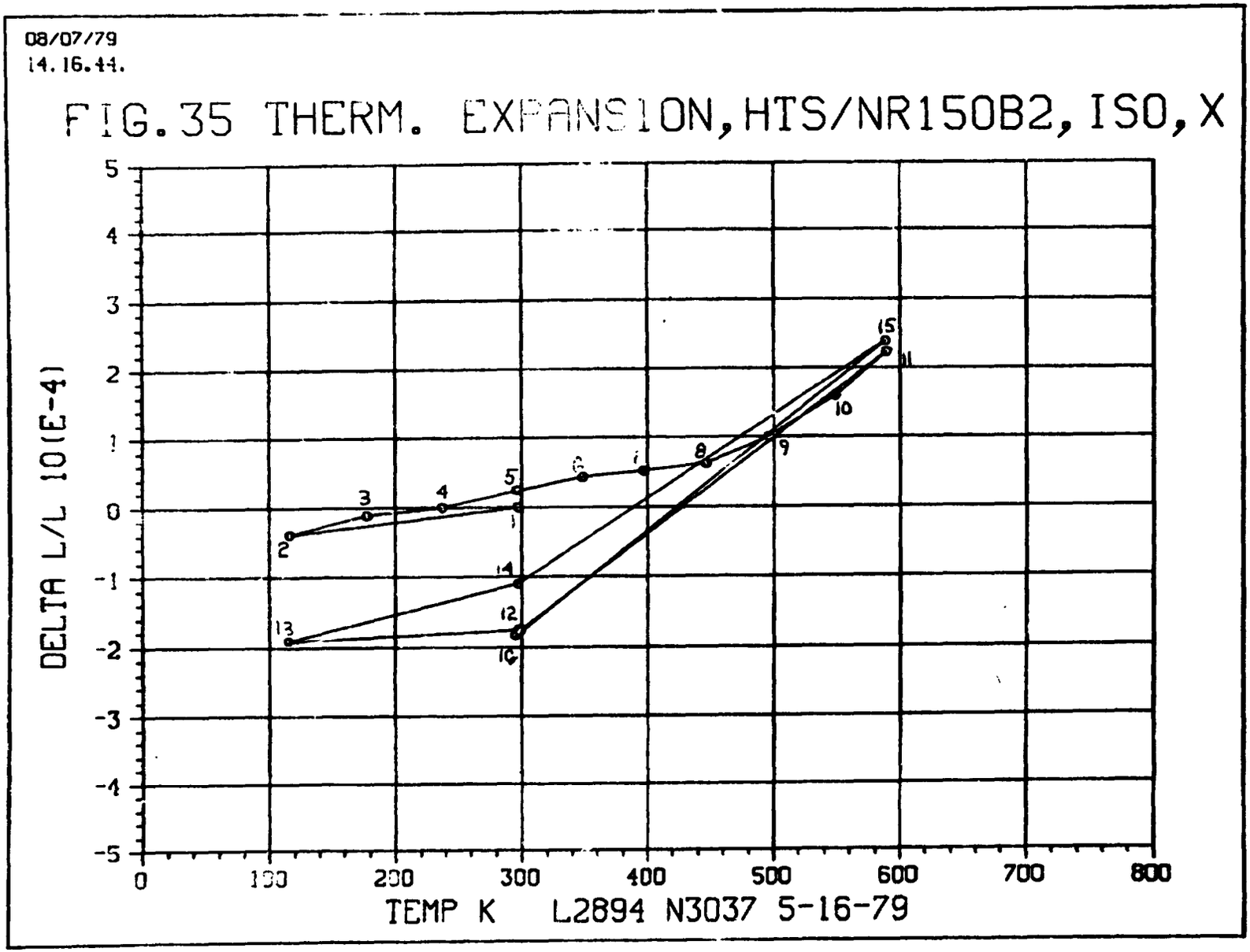
08/07/79
14.16.44.
FIG.35 THERM. EXPANSION, HTS/NR150B2, ISO, X
DELTA L/L 10(E-4)
5
4
3
2
1
0
-1
-2
-3
-4
-5
0
100
200
300
400
500
600
700
800
TEMP K
L2894 N3037 5-16-79
1
2
3
4
5
6
7
8
9
10
11
12
13
14
15
16

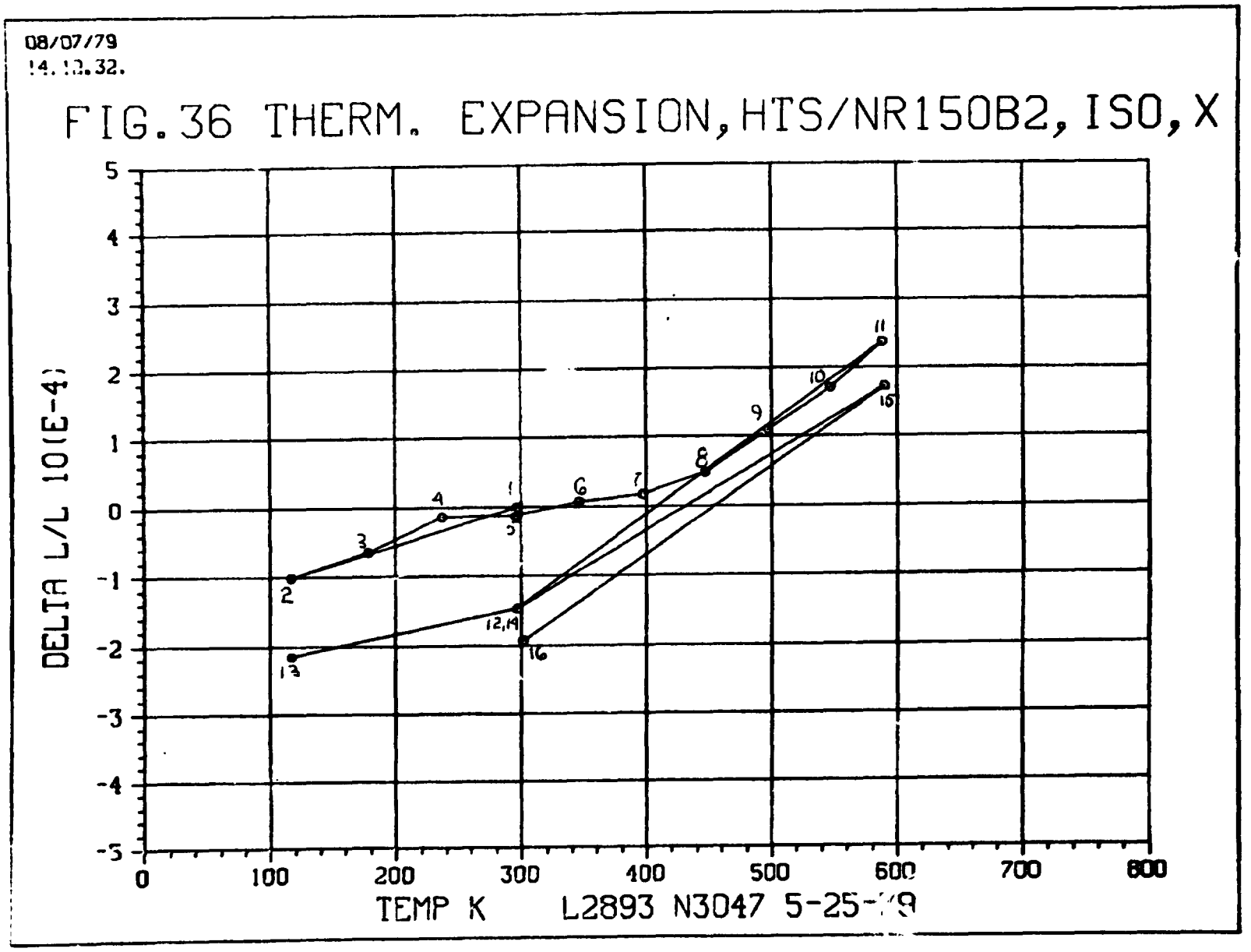
08/07/79
14.10.32.
FIG.36 THERM. EXPANSION, HTS/NR150B2, ISO, X
DELTA L/L 10(E-4)
5
4
3
2
1
0
-1
-2
-3
-4
-5
0
100
200
300
400
500
600
700
800
TEMP K
L2893 N3047 5-25-79

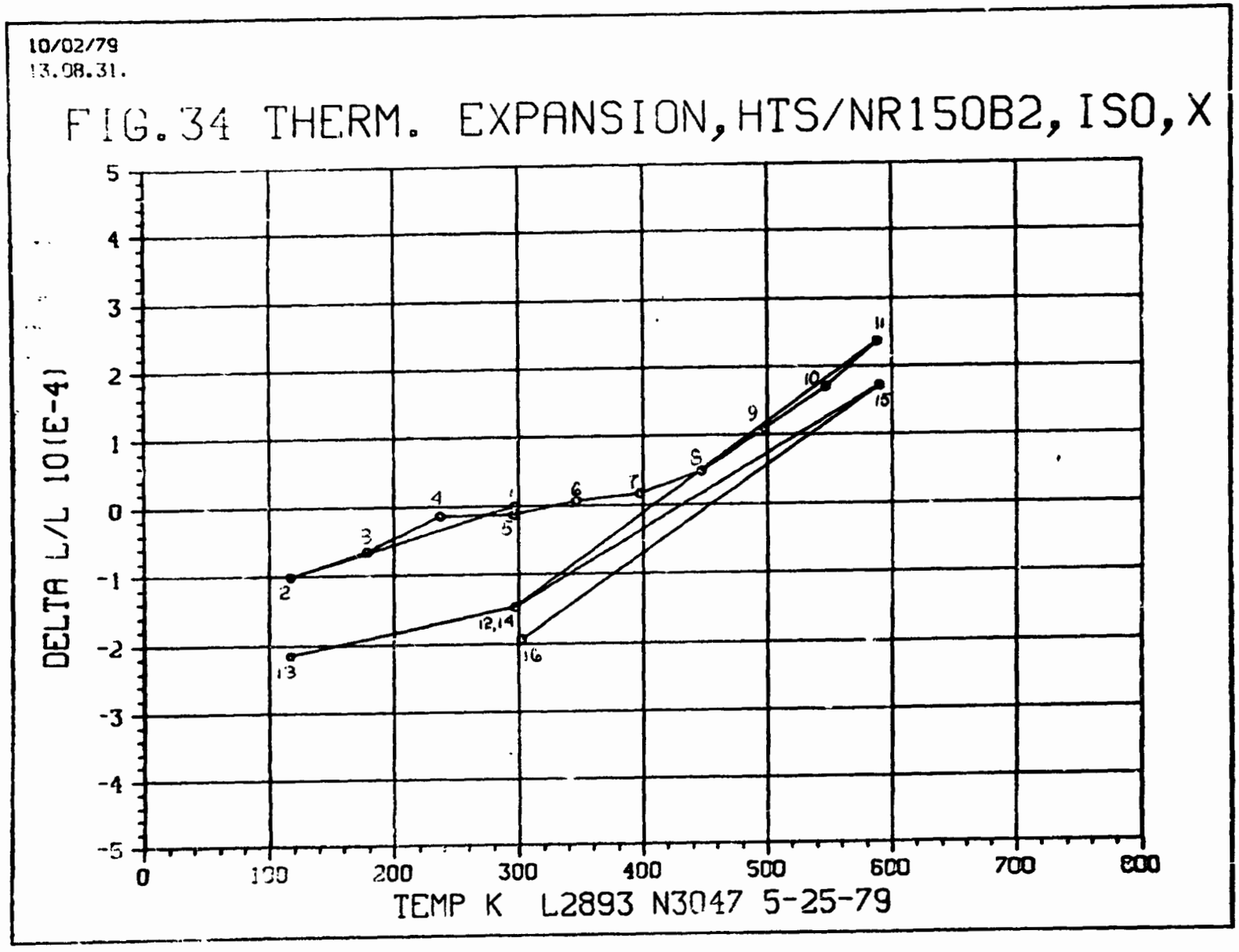
10/02/79
13.08.31.
FIG.34 THERM. EXPANSION, HTS/NR150B2, ISO, X
DELTA L/L 10(E-4)
TEMP K L2893 N3047 5-25-79
5
4
3
2
1
0
-1
-2
-3
-4
-5
0
100
200
300
400
500
600
700
800
2
3
4
5
6
7
8
9
10
11
12,14
13
15
16

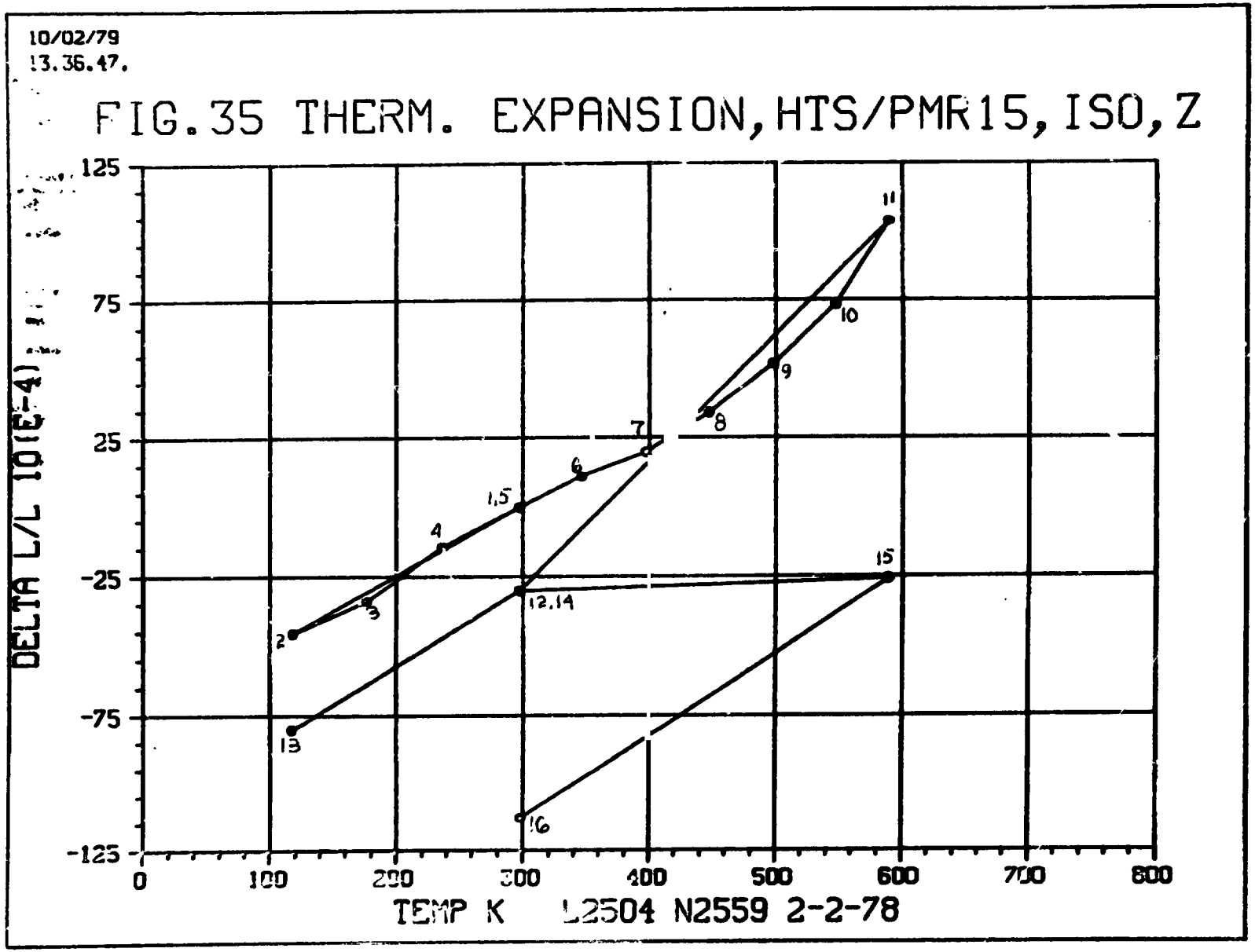
10/02/79
13.36.47.
FIG.35 THERM. EXPANSION, HTS/PMR15, ISO, Z
DELTA L/L 10(E-4)
125
75
25
-25
-75
-125
0
100
200
300
400
500
600
700
800
TEMP K
L2504 N2559 2-2-78
1
2
3
4
5
6
7
8
9
10
11
12,14
13
15
16

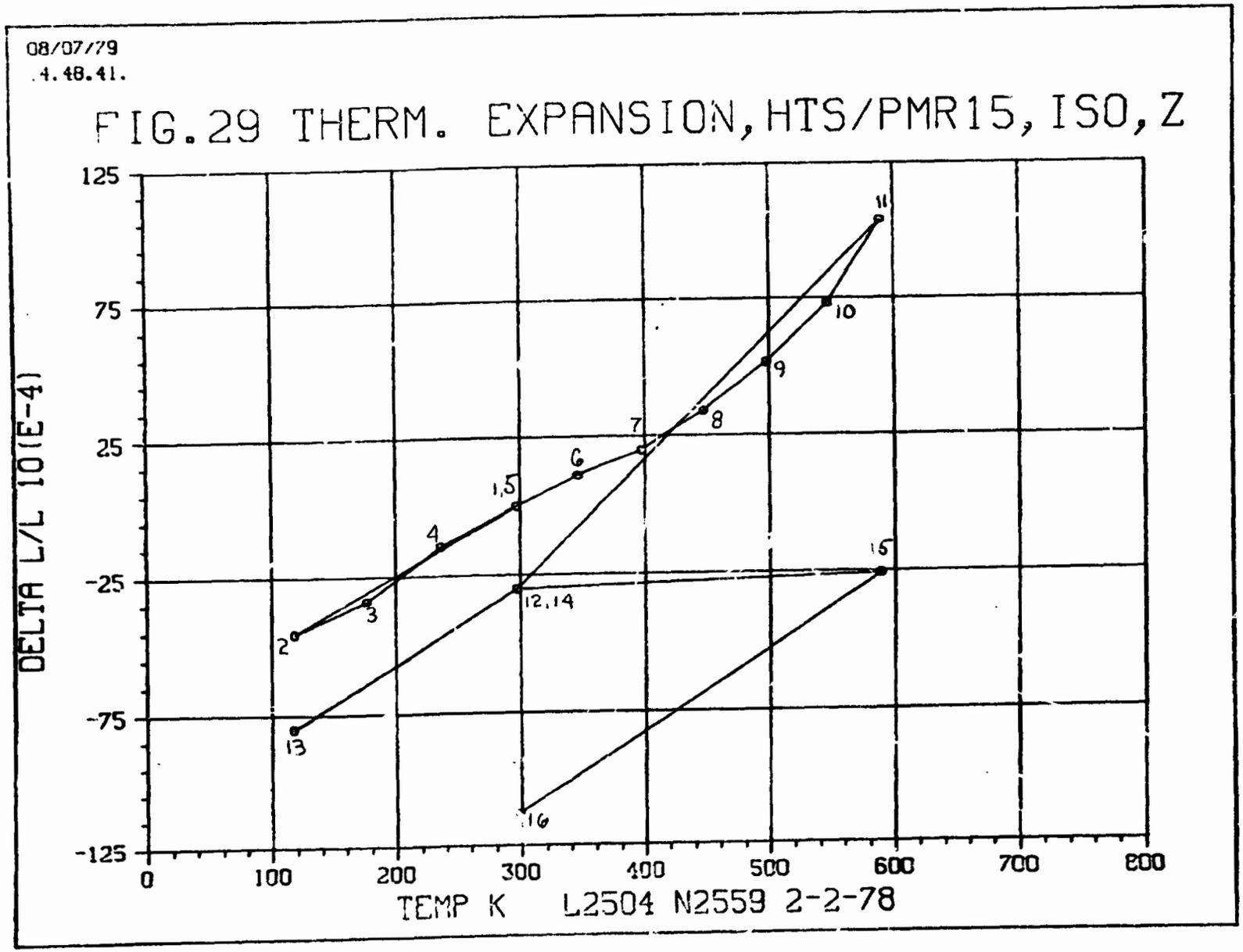
08/07/79
.4.48.41.
FIG.29 THERM. EXPANSION, HTS/PMR15, ISO, Z
DELTA L/L 10(E-4)
125
75
25
-25
-75
-125
0
100
200
300
400
500
600
700
800
TEMP K L2504 N2559 2-2-78
1
1,5
2
3
4
5
6
7
8
9
10
11
12,14
13
16

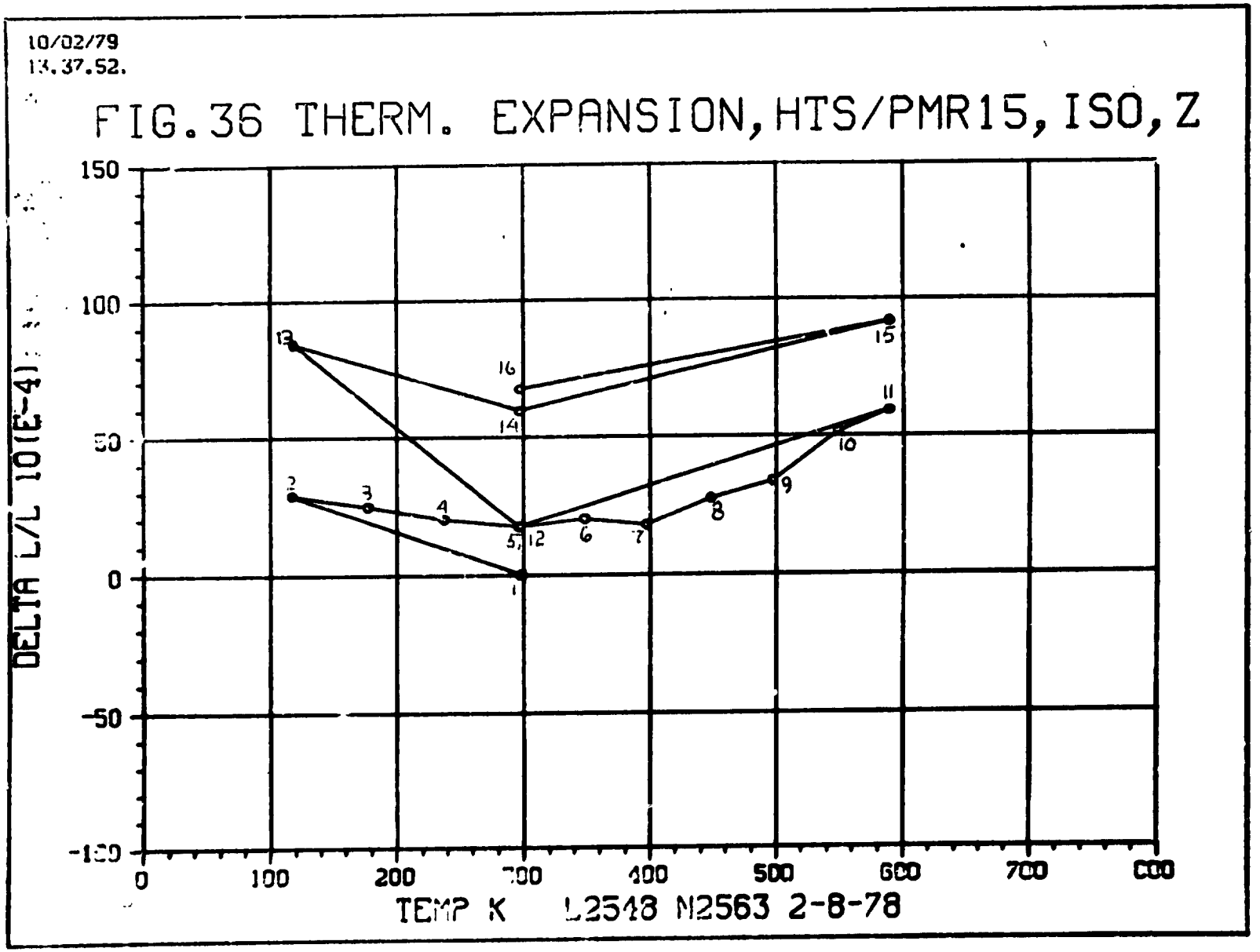
10/02/79
13.37.52.
FIG.36 THERM. EXPANSION, HTS/PMR15, ISO, Z
DELTA L/L 10(E-4)
150
100
50
0
-50
-100
0
100
200
300
400
500
600
700
800
TEMP K
L2548 N2563 2-8-78
1
2
3
4
5
6
7
8
9
10
11
12
13
14
15
16

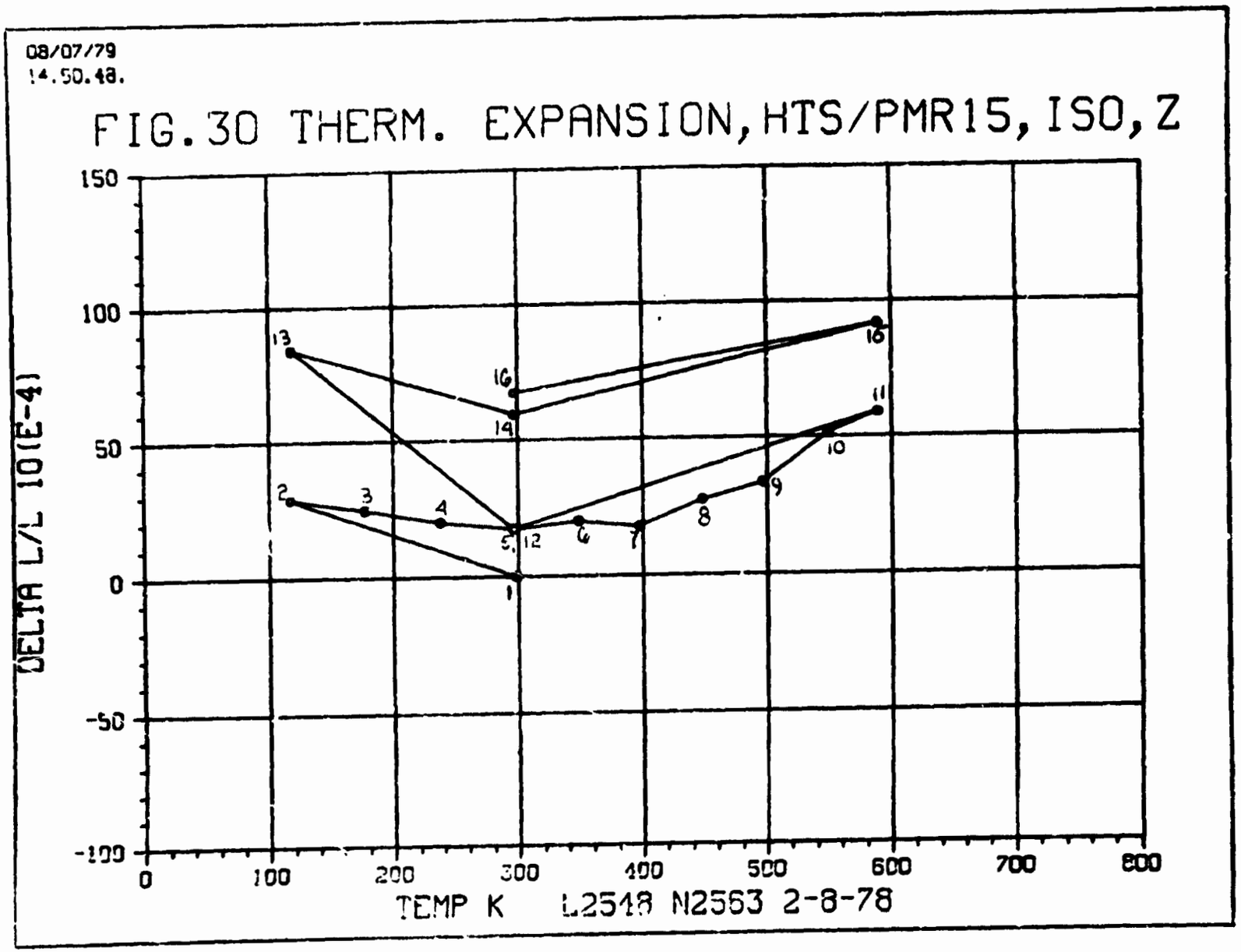
08/07/79
14.50.48.
FIG.30 THERM. EXPANSION, HTS/PMR15, ISO, Z
DELTA L/L 10(E-4)
150
100
50
0
-50
-100
0
100
200
300
400
500
600
700
800
TEMP K L2518 N2563 2-8-78
1
2
3
4
5
6
7
8
9
10
11
12
13
14
15
16

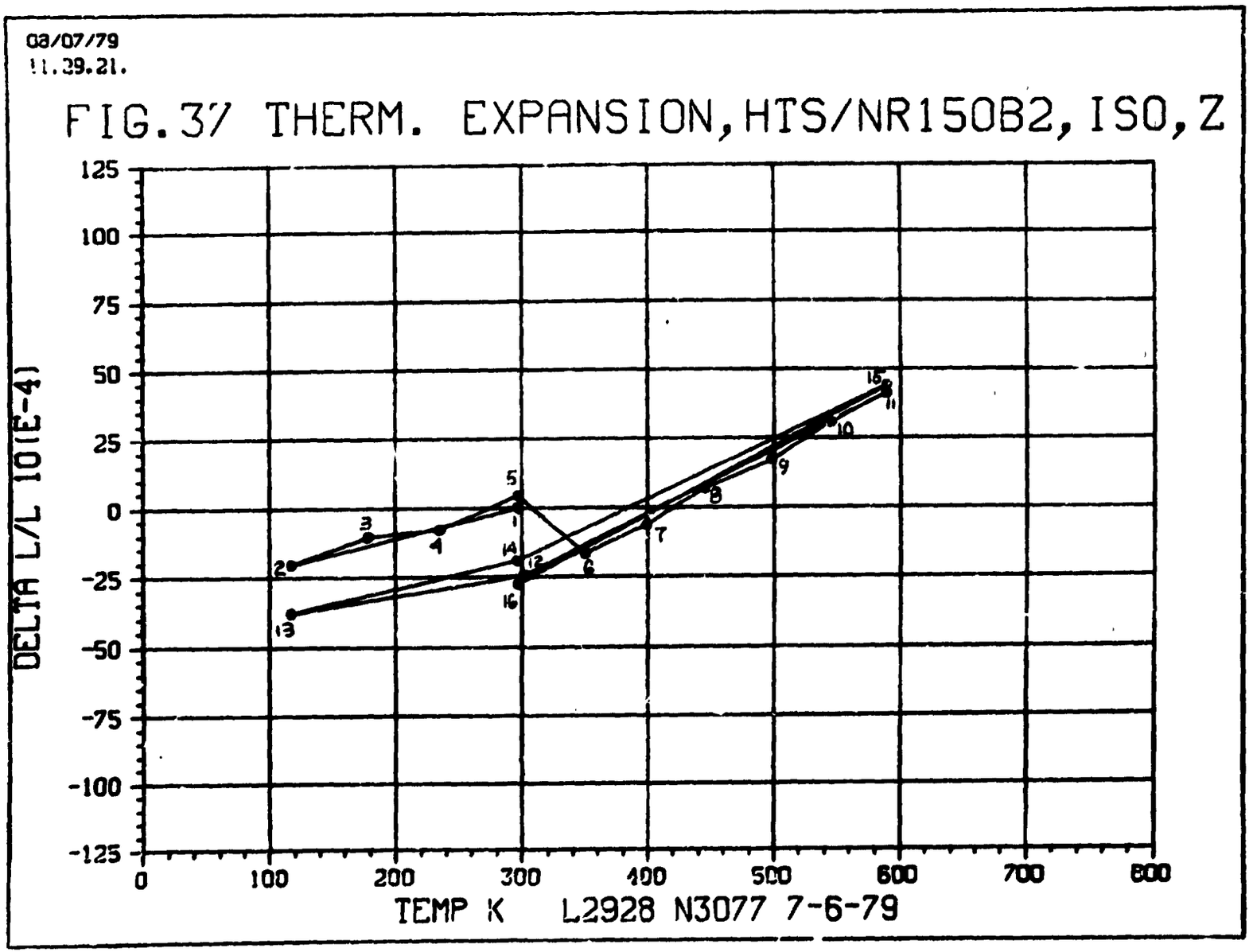
08/07/79
11.39.21.
FIG.37 THERM. EXPANSION, HTS/NR150B2, ISO, Z
DELTA L/L 10(E-4)
125
100
75
50
25
0
-25
-50
-75
-100
-125
0
100
200
300
400
500
600
700
800
TEMP K
L2928 N3077 7-6-79

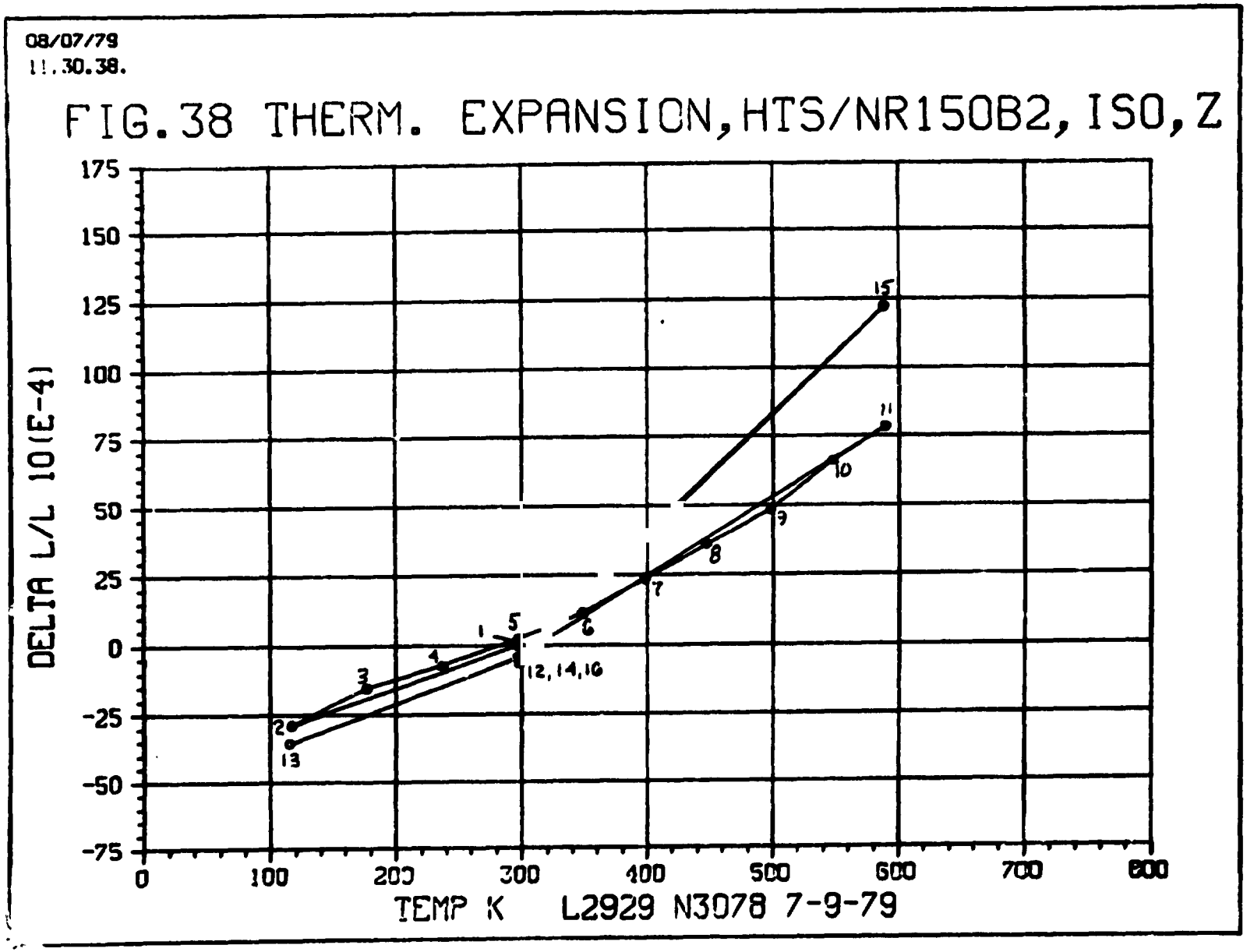
08/07/79
11.30.38.
FIG.38 THERM. EXPANSION,HTS/NR150B2, ISO,Z
DELTA L/L 10(E-4)
175
150
125
100
75
50
25
0
-25
-50
-75
0
100
200
300
400
500
600
700
800
TEMP K
L2929 N3078 7-9-79
1
2
3
4
5
6
7
8
9
10
11
12,14,16
13
15

Emittance

Emittance results for both materials are given in Table 4. In all cases, values for the HTS/NR 150B2 specimens were slightly higher than those for the HTS/PMR 15 specimens. Emittance data at 589K for both materials, are approximately 3% higher than those at 300K.

Table 4. Emittance Results

	Emittance	
	300K	589K
HTS/PMR 15-1	.85	.87
-2	.83	.86
HTS/NR 150B2-1	.88	.91
-2	.87	.90

CONCLUSIONS

Following are conclusions which can be drawn from the test results for each property.

Thermal Conductivity

Thermal conductivities of HTS/PMR 15 and HTS/NR 150B2 are very similar in the isotropic Z and unidirectional Y direction where the resin properties dominate.

Significant differences between the two materials were observed in the unidirectional X and isotropic X directions where the fiber properties dominate. It is suspected that the differences result from the higher void content of the HTS/NR150B2 contributing to artifically low test results.

Thermal Expansion

Scatter was high and reproducibility was poor for both materials leading to the conclusion that laminate quality when compared to those for lower temperature resin systems, was not optimum in either case.

Higher expansion of the PMR 15 laminates in all except the unidirectional X direction where the fiber dominates, indicates a higher coefficient for PMR 15 than NR 150B2.

Specific Heat

Differencies between specific heats for the two materials were expected due to differences in structures of the resins. Values for the HTS/PMR 15 specimens were consistently higher than those for the HTS/NR 150B2 specimens with the difference being approximately 4% at 300K.

Emittance

Values for the HTS/NR 150B2 samples were approximately 4% higher than those for HTS/PMR 15. In both cases, 589K results were approximately 3% higher than the results at 300K.

APPENDIX

Tabular Test Data

TABLE A-1. CONDUCTIVITY TEST DATA

TEMPERATURE (K)	CONDUCTIVITY (W)/(MK)	TEMPERATURE (K)	CONDUCTIVITY (W)/(MK)
FIGURE 15		FIGURE 18	
125	8.33	115	0.28
175	12.7	172	0.33
244	18.1	231	0.47
306	21.6	312	0.57
372	27.1	369	0.65
440	29.2	434	0.79
501	35.5	502	0.88
583	41.9	583	0.85
FIGURE 16		FIGURE 19	
106	0.51	147	3.87
183	0.85	169	4.63
249	0.93	195	5.29
311	0.93	296	7.57
393	1.02	367	9.46
443	1.16	432	11.4
503	1.34	575	14.4
591	1.39		
FIGURE 17		FIGURE 20	
120	3.76	138	0.47
180	6.58	176	0.60
246	8.13	240	0.78
309	9.93	326	0.86
375	11.2	377	0.99
437	12.1	447	1.09
497	13.7	506	1.20
581	15.1	597	1.33

TABLE A-1. (continued)

TEMPERATURE (K)	CONDUCTIVITY (W)/(MK)	TEMPERATURE (K)	CONDUCTIVITY (W)/(MK)
FIGURE 21		FIGURE 22	
189	2.22	102	0.37
262	3.76	178	0.33
314	4.76	244	0.47
362	5.59	312	0.55
418	6.72	376	0.59
477	7.92	442	0.73
523	9.60	500	0.81
		596	0.87

TABLE A-2. EXPANSION TEST DATA

TEMP (K)	EXPANSION ($\Delta L/L \times 10^{-4}$)	TEMP (K)	EXPANSION ($\Delta L/L \times 10^{-4}$)	TEMP (K)	EXPANSION ($\Delta L/L \times 10^{-4}$)
	FIGURE 23		FIGURE 25		FIGURE 27
297	0.00	298	0.00	297	0.0
117	0.63	116	0.78	117	-36.5
177	0.26	177	0.60	175	-26.3
236	-0.03	235	0.31	236	-13.9
297	0.00	296	0.15	297	0.00
347	-0.43	347	-0.25	348	14.5
397	-0.49	397	-0.72	397	28.3
448	-0.31	450	-0.76	447	42.5
499	-0.16	498	-0.63	497	56.1
549	0.49	547	-0.28	552	70.1
300	-0.91	589	0.00	590	78.9
118	0.68	297	-1.45	293	-14.4
297	0.00	115	-0.20	117	-50.4
569	0.36	297	-0.92	297	-14.4
297	-1.12	589	0.13	590	71.5
		297	-1.48	297	-16.4
	FIGURE 24		FIGURE 26		FIGURE 28
297	0.00	297	0.00	298	0.0
116	0.50	117	0.59	118	-37.4
166	0.36	178	0.53	175	-27.0
235	0.28	237	0.18	237	-14.1
297	0.00	297	-0.03	298	0.00
348	-0.32	347	-0.17	347	13.3
397	-0.48	402	-0.52	399	29.2
448	-0.67	446	-0.76	447	43.5
497	-0.59	499	-0.69	498	59.8
555	-0.55	551	-0.62	551	71.7
588	-0.57	589	-0.45	590	78.8
297	-0.51	297	-1.28	297	-14.8
117	0.14	117	-0.25	117	-52.1
298	-0.49	298	-1.08	293	-22.1
589	-1.67	589	-0.28	589	67.2
297	-1.93	297	-1.90	298	-22.0

Table A-2 (continued)

TEMP (K)	EXPANSION ($\Delta L/L \times 10^{-4}$)	TEMP (K)	EXPANSION ($\Delta L/L \times 10^{-4}$)	TEMP (K)	EXPANSION ($\Delta L/L \times 10^{-4}$)
	FIGURE 29		FIGURE 31		FIGURE 33
297	0.0	292	0.00	297	0.00
118	-22.7	118	-1.40	116	-0.38
178	-17.2	177	-0.85	177	-0.11
235	- 9.00	236	-0.28	237	0.00
297	0.05	292	0.26	236	0.25
347	8.70	348	0.56	348	0.43
398	16.7	297	-1.93	396	0.52
451	25.8	397	0.89	446	0.62
497	32.4	448	1.17	496	1.01
547	42.7	499	1.89	549	1.60
589	55.3	552	2.92	589	2.23
298	1.90	589	3.58	299	-1.76
117	-20.0	291	-0.53	115	-1.91
297	5.50	118	-1.84	297	-1.10
589	61.9	291	-0.58	583	2.38
298	5.30	590	1.77	295	-1.84
		296	-3.61		
	FIGURE 30		FIGURE 32		FIGURE 34
298	0.00	297	0.00	297	0.00
116	-25.3	116	-1.59	117	-1.01
177	-19.4	175	-0.94	178	-0.65
237	-10.6	237	-0.44	237	-0.14
297	- 0.50	298	0.00	296	-0.13
348	7.70	347	-0.61	346	0.07
407	17.5	397	-0.53	397	0.17
447	24.6	448	-0.08	447	0.49
498	34.5	498	0.79	497	1.10
546	45.1	548	1.50	547	1.71
589	54.5	586	2.13	583	2.37
297	1.20	295	-2.44	297	-1.47
115	-24.4	114	-3.44	117	-2.15
297	0.90	297	-4.07	297	-1.47
589	58.3	588	0.42	590	1.72
298	- 0.70	297	-3.96	302	-1.93

TABLE A-2. (continued)

TEMP (K)	EXPANSION ($\Delta L/L \times 10^{-4}$)	TEMP (K)	EXPANSION ($\Delta L/L \times 10^{-4}$)	TEMP (K)	EXPANSION ($\Delta L/L \times 10^{-4}$)
	FIGURE 35		FIGURE 37		FIGURE 38
297	0.00	297	0.00	297	0.00
118	-45.4	117	-20.4	117	-28.9
176	-33.8	178	-10.4	177	-15.2
236	-14.3	235	- 7.80	237	- 7.25
297	0.00	297	4.20	297	2.08
346	11.1	350	-16.5	348	11.1
397	20.0	399	- 6.20	398	23.5
447	34.4	445	6.70	447	35.8
498	51.9	498	17.1	498	48.2
547	73.0	545	30.8	548	65.9
589	103.0	589	41.2	589	78.3
297	-30.0	302	-24.3	297	- 4.60
117	-80.1	117	-37.9	115	-35.6
297	-30.0	296	-19.2	298	- 4.60
589	-25.7	589	43.9	588	122.0
298	-112.0	297	-27.6	298	- 6.40
	FIGURE 36				
298	0.00				
117	29.1				
177	25.1				
237	20.3				
297	17.6				
348	20.3				
397	18.1				
448	27.6				
497	33.8				
549	51.6				
589	59.2				
296	17.6				
118	84.3				
297	59.6				
589	91.4				
297	67.4				

TABLE A-3. SPECIFIC HEAT TEST DATA

TEMPERATURE (K)	SPECIFIC HEAT
	FIGURE 39
116	.285
181	.440
245	.615
310	.808
374	.959
439	1.11
503	1.22
589	1.36
	FIGURE 40
116	.168
181	.419
245	.608
310	.775
374	.943
439	1.05
503	1.13
589	1.24

1. Report No.	2. Government Accession No.	3. Recipient's Catalog No.
NASA CR-159164		

4. Title and Subtitle	5. Report Date
Thermophysical Properties Data on Graphite/Polyimide Composite Materials	November, 1979
	6. Performing Organization Code
7. Author(s)	8. Performing Organization Report No.
M. D. Campbell and D. D. Burleigh	GDC-NAS-79-002
	10. Work Unit No.
9. Performing Organization Name and Address	11. Contract or Grant No.
General Dynamics Convair Div. P.O. Box 80847, MZ 43-6332 San Diego, CA 92138	NAS1-15103
	13. Type of Report and Period Covered
12. Sponsoring Agency Name and Address	Contractor Report (Final)
National Aeronautics and Space Administration Washington, D.C. 20546	14. Army Project No.

15 Supplementary Notes

Contract Monitor: Dr. Ronald K. Clark, NASA Langley Research Center

16 Abstract

Experimental data for the thermal conductivity, thermal expansion, specific heat, and emittance of [0] and $[0, 45, 90, 135]_S$ laminates of HTS/NR 150B2 and HTS/PMR 15 are presented. Measurements were made over the temperature range 116K to 588K (-250F to 600F).

Results for the two materials were similar with some differences attributable to laminate quality. Higher expansion coefficients for the HTS/PMR 15 specimens in the resin-dominated directions indicate a higher coefficient for PMR 15 than NR 150B2.

17. Key Words (Suggested by Author(s))	18. Distribution Statement
Thermophysical Properties Graphite/Polyimide Composites	Unclassified - Unlimited

19. Security Classif. (of this report)	20. Security Classif. (of this page)	21. No. of Pages	22. Price*
Unclassified	Unclassified	66	

*For sale by the National Technical Information Service, Springfield, Virginia 22161